1 μmol/L EDTA (pH 7.6)] supplemented with protease inhibitor cocktail Complete Mini (Roche Diagnostics). After centrifugation of the homogenates (3000*g* for 10 minutes), the supernatants or serum samples were used for measurement. To activate latent TGF-β_1 to an immunoreactive form, the samples were treated with acid according to the manufacturer's instructions (R&D Systems Inc). IL-10 or IL-6 concentrations in the sera and TGF-β_1, IL-6, HO-1, or TNF-α in the lung extracts were measured using enzyme-linked immunosorbent assay (ELISA) kits (Amersham Pharmacia Biotech; R&D Systems). The minimum detectable dose was 3, 3, 16, and 5 pg/mL or 0.78 ng/mL for IL-10, TGF-β_1, IL-6, and TNF-α, or HO-1, respectively. Inter- and intraassay precision of these kits was <10%. The total protein concentrations in the lung extracts were estimated using a BCA Protein Assay kit (PIERCE). The levels of TGF-β_1, IL-6, HO-1, or TNF-α in the lung were expressed as pg per mg protein.

Cell Culture and Proliferation Assay

Human PASMCs were obtained from Clonetics Corp and grown in SmGM-2 medium (Clonetics Corp). PASMCs with a passage between 4 and 6 were used in the experiments. Cells (1×10^3 per well) were incubated in 96-well plates with serum-free Dulbecco's modified Eagle's medium and nutrient mixture F12 (DMEM-F12, Invitrogen) in an atmosphere of 5% CO_2 in the air at 37°C. A tetrazolium-based colorimetric proliferation assay (XTT assay; Cell Proliferation Kit II, Roche Diagnostics) was performed 2 days after adding tin protoporphyrin IX (SnPP; Frontier Scientific), human recombinant TGF-β_1, IL-6, or IL-10 (PeproTech Inc). The optical density between 450 and 650 nm were measured to estimate the number of viable cells.

Statistical Analysis

Data from multiple experiments are expressed as mean±SEM. Statistical analysis and correlations were performed using StatView (Abacus Concepts, Inc). Survival curves were analyzed using the Kaplan–Meier method and compared by log-rank tests. Differences in other parameters were evaluated by analysis of variance combined with Fisher test. The correlation test was used to measure the association between 2 variables. A value of $P<0.05$ was considered statistically significant.

Results

AAV Vector-Mediated IL-10 Expression Improves Survival of MCT-PAH Rats

Eight weeks after AAV-IL-10 injection, serum IL-10 concentrations were elevated in a vector dose-dependent manner (Figure 1A). We determined that injection with AAV-IL-10 (6×10^{10} g.c. per rat) significantly increased serum IL-10 levels as compared with untreated controls (184.1±47.6 versus 18.8±1.3 pg/mL, $P<0.05$, n=3 each). In contrast, injection with MCT (Figure 1A) or AAV-eGFP alone (data not shown) caused no significant change in serum IL-10 levels. Therefore, we used this dosage for all vectors in subsequent experiments. For survival analysis, the rats were injected with a lethal dose of MCT, after 4 weeks of vector injection. The survival in IL-10–transduced rats was significantly improved as compared with the eGFP-transduced rats 8 weeks after MCT injection (75% versus 0%, $P<0.01$, n=8 each; Figure 1B).

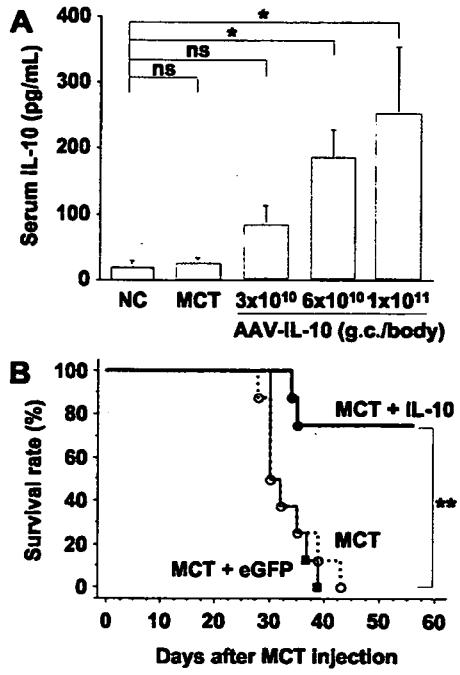

Figure 1. Adeno-associated virus (AAV) vector-mediated systemic interleukin (IL)-10 expression improves survival of monocrotaline (MCT)-induced pulmonary arterial hypertension (PAH) rats. A, In vivo IL-10 expression induced by AAV-IL-10. Serum IL-10 concentrations (pg/mL) were determined using ELISA 8 weeks after a single intramuscular injection of AAV-IL-10 into the anterior tibial muscles of 3-week-old Wistar rats. Genome copies (g.c.) per rat were as indicated. Data represent mean±SEM (n=3 animals per group, *$P<0.05$). ns indicates not statistically significant; NC, untreated controls. B, The Kaplan-Meier survival curve in MCT-PAH rats. The Wistar rats were treated with a lethal dose of MCT 4 weeks after the single intramuscular injection of HN buffer (MCT group), AAV-eGFP (MCT+eGFP group), or AAV-IL-10 (MCT+IL-10 group). n=8 animals per group, **$P<0.01$ versus MCT or MCT+eGFP groups.

Effects of IL-10 on PAH and RVH

Four weeks after MCT injection, the mPAP levels were significantly higher than those of the untreated controls (30.1±4.0 versus 20.0±2.1 mm Hg, $P<0.01$, n=5 each; Figure 2A). Treatment with AAV-IL-10 but not AAV-eGFP significantly inhibited the elevation of mPAP (22.8±1.5 versus 29.7±2.8 mm Hg, $P<0.01$, n=5 each; Figure 2A). Moreover, serum IL-10 concentrations correlated negatively with mPAP in MCT-treated rats ($r=-0.75$, $P<0.01$, n=15; Figure 2B). In contrast, this IL-10 expression caused no significant change in HR (data not shown) and mAoP (76.7±2.1 versus 74.6±6.8 mm Hg, MCT+IL-10 versus MCT+eGFP group, n=5 each). IL-10 expression also has a beneficial effect on RVH. Four-week MCT treatment significantly increased the RV/(LV+S) values as compared with the untreated controls ($P<0.01$, n=5 each; Figure 2C). Treatment with AAV-IL-10 but not AAV-eGFP inhibited MCT-induced increase of RV/(LV+S) significantly ($P<0.05$, n=5 each; Figure 2C). Furthermore, serum IL-10 concentrations correlated negatively with RV/(LV+S) in MCT-treated rats ($r=-0.57$, $P<0.05$, n=15; Figure 2D). These results indicate that sustained IL-10 expression prevented the development of MCT-induced PAH and RVH.

Effects of IL-10 on Histological Changes of the PA

Medial hypertrophy is a hallmark of pathological vascular remodeling in PAH. Four weeks after MCT injection, the medial thickness of PAs was markedly increased in the MCT-treated rats compared with untreated controls ($P<0.01$,

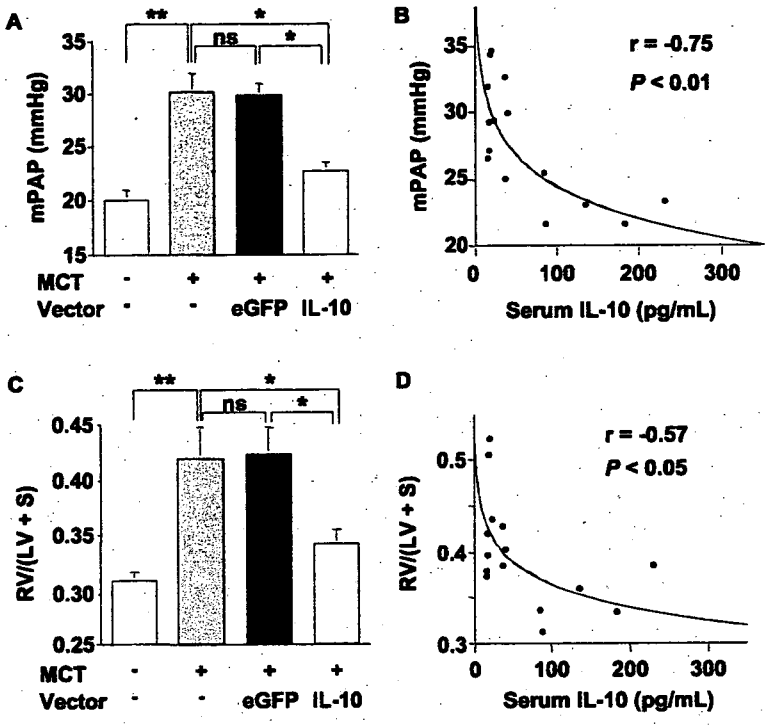

Figure 2. Effects of IL-10 on PAH and right ventricular hypertrophy (RVH). The 7-week-old Wistar rats were treated with monocrotaline (MCT) 4 weeks after vector injection. A, Statistical analysis of mean pulmonary arterial pressure (mPAP, mm Hg) determined by direct catheterization 4 weeks after MCT injection. Data represent the mean±SEM (n=5 animals per group; $^*P<0.05$, $^{**}P<0.01$). ns indicates not statistically significant. B, Correlation between serum IL-10 concentrations and mPAP levels in the MCT-treated rats (groups: MCT, MCT+eGFP, or MCT+IL-10; n=5 animals per group; $r=-0.75$, $P<0.01$). C, Quantitative RVH analysis. The weight ratio of the right ventricle to left ventricle plus septum [RV/(LV+S)] is presented as an index of RVH (n=5 animals per group; $^*P<0.05$, $^{**}P<0.01$). D, Correlation between serum IL-10 concentrations and RV/(LV+S) in the MCT-treated rats (groups: MCT, MCT+eGFP, and MCT+IL-10; n=5 animals per group; $r=-0.57$, $P<0.05$).

n=5 each; Figure 3B, 25 to 50 μm; Figure 3C, 51 to 100 μm in external diameter). Treatment with AAV-IL-10 but not AAV-eGFP significantly inhibited the increase in percent medial thickness ($P<0.01$, n=5 each). Inflammatory cell infiltration and vascular cell proliferation are also important indicators in the progression of PA remodeling. Immunohistochemical analysis shows that treatment with AAV-IL-10 significantly decreased the number of accumulated macrophages (ED1-positive cells; $P<0.01$, n=5 each; Figure 3D) and proliferating vascular cells (PCNA-positive cells; $P<0.01$, n=5 each; Figure 3E) in the PA of MCT-treated rats as compared with treatment with MCT alone or AAV-eGFP.

Effects of IL-10 on Cytokine Expression

We analyzed pulmonary tissue and serum cytokine levels relevant to the pathogenesis of PAH. Four weeks after MCT injection, the TGF-β_1 and IL-6 levels in the MCT-treated rats were significantly higher than those of the untreated controls ($P<0.01$, n=5 each; Figure 4A and 4C). Treatment with AAV-IL-10 but not AAV-eGFP significantly inhibited the MCT-induced elevation of TGF-β1 and IL-6 levels ($P<0.01$, n=5 each). Furthermore, these levels correlated positively with the percent medial thickness in the rats with or without MCT treatment ($r=0.84$, $P<0.01$; $r=0.87$, $P<0.01$, respectively; Figure 4B and 4D).

HO-1 has been reported to mediate the antiinflammatory effects of IL-10.[24] Treatment with AAV-IL-10 but not AAV-eGFP or MCT alone significantly increased the lung HO-1 levels as compared with untreated controls ($P<0.05$, n=5 each, Figure 4E). In addition, HO-1 levels correlated negatively with IL-6 levels in MCT-treated rats ($r=-0.85$, $P<0.01$; Figure 4F). In contrast, serum IL-6 levels positively correlated with lung IL-6 levels ($r=-0.69$, $P<0.01$; Figure 4G). Although the lung TNF-α levels significantly increased in MCT-treated rats compared with untreated controls, IL-10 expression caused no change in the lung TNF-α levels (Figure 4H).

Effects of IL-10 on PASMC Proliferation

To determine whether IL-10 directly inhibits PASMC proliferation, we performed an in vitro colorimetric XTT assay using cultured human PASMCs. Treatment of PASMCs with SnPP, which inactivates HO-1, and treatment with TGF-β_1 or IL-6 dose dependently promoted cell proliferation (n=4 each, $P<0.05$; Figure 5A through 5C). Treatment with IL-10 alone had no significant effect on PASMC proliferation (Figure 5D). On the other hand, pretreatment with IL-10 significantly inhibited PASMC proliferation induced by SnPP or TGF-β_1 (n=4 each, $P<0.05$; Figure 5E) but not that induced by IL-6.

Discussion

The present study demonstrates that IL-10, delivered by an intramuscular injection of an AAV1 vector, prevented the development of MCT-PAH in rats. Systemic IL-10 expression also improved survival in rats and prevented the development of RVH and medial hypertrophy of PA. IL-10 also reduced macrophage accumulation, vascular cell proliferation, and pulmonary tissue levels of TGF-β_1 and IL-6, all of which play pivotal roles in progression of PA remodeling. Further, IL-10 enhanced HO-1 levels in the lung. Thus, IL-10 exerts multiple preventive effects on inflammatory and proliferative PA remodeling (Figure 6).

Blockade of a single proinflammatory signaling pathway by IL-1 or monocyte chemoattractant protein-1 attenuates PA remodeling.[25,26] However, the prosurvival effects of antiinflammatory molecules on PAH animals have not been re-

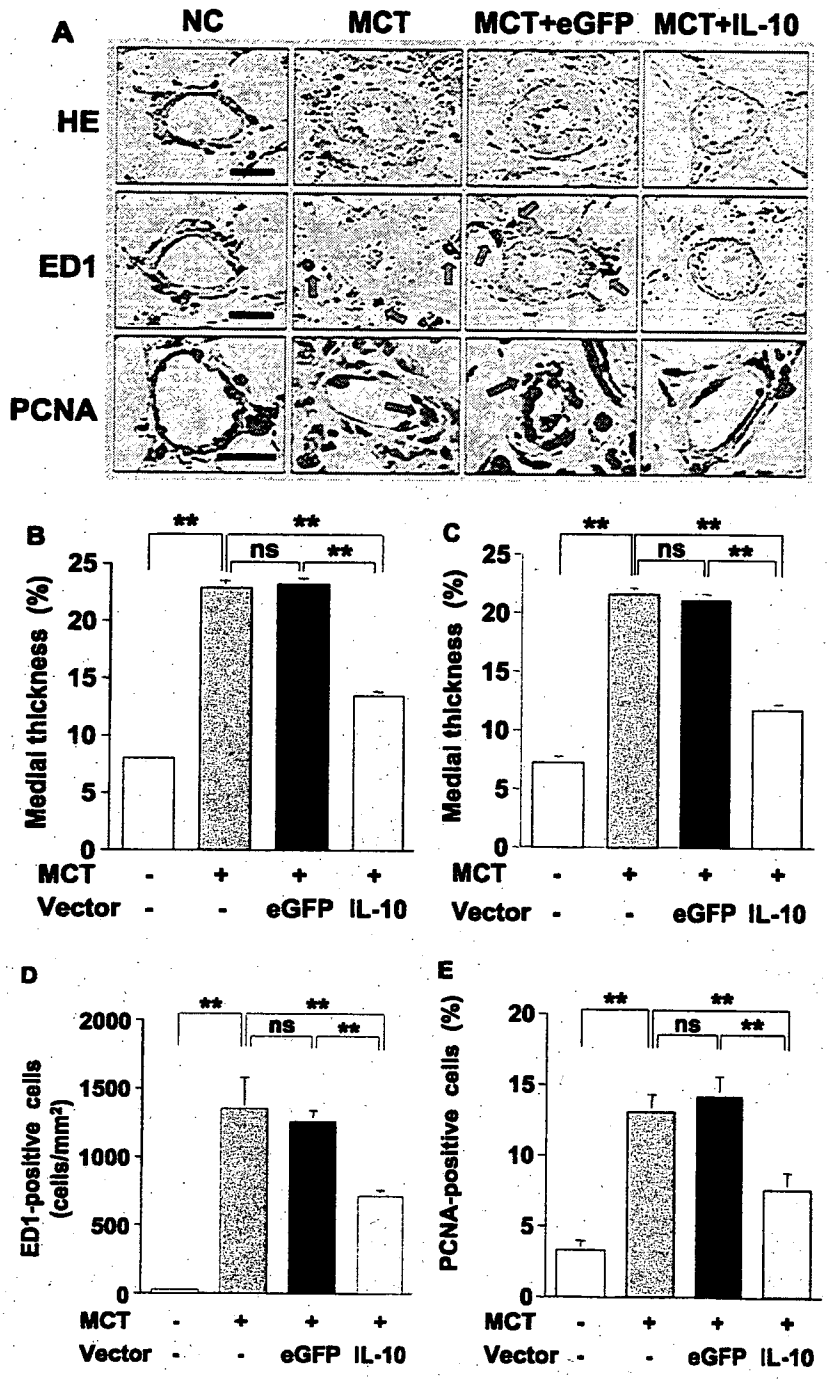

Figure 3. Antiinflammatory and antiproliferative effects of IL-10 on the remodeled pulmonary artery (PA). The 7-week-old Wistar rats were treated with MCT 4 weeks after vector injection. Representative cross-sectional views of the peripheral PAs stained with HE or immunohistochemistry (ED1 or PCNA) 4 weeks after MCT treatment (A; original magnification ×1000, Scale bar=20 μm). Blue arrows indicate ED-1–positive cells and red arrows, PCNA-positive cells. Quantification of percent medial thickness for vessels 25 to 50 μm (B) and 51 to 100 μm (C) in external diameter. Quantitative analysis of the number of perivascular macrophages (ED-1–positive cells, D) and proliferating vascular cells (PCNA-positive cells, E). Data represent mean±SEM (n=5 animals per group, $^{**}P<0.01$). ns indicates not statistically significant.

ported. Evidence of right heart failure is involved in the mortality of MCT-PAH rats. In this study, all rats treated with a lethal dose of MCT exhibited symptoms of right heart failure such as pleural effusion and body weight decrease. In the setting of severe PAH and right heart failure, cytokine networks may orchestrate disease progression. Thus, blockades of multiple inflammatory signals might be responsible for the prosurvival effect of IL-10.

IL-10 has gained significant attention because of its suppressive influence on inflammatory and proliferative vasculopathy. The IL-10 receptor is expressed on vascular smooth muscle cells (VSMCs). IL-10 inhibits inflammation and VSMC proliferation in arterial remodeling after balloon injury or transplant rejection.[12,13] Consistent with previous studies using MCT-PAH,[6,7] we demonstrate that increased levels of TGF-β_1 and IL-6 are related to PASMC proliferation and PA remodeling progression. Although treatment with IL-10 alone caused no significant effects on PASMC proliferation,[27] IL-10 significantly inhibited the lung TGF-β_1 expression and TGF-β_1-induced PASMC proliferation. TGF-β_1 enhances PASMC proliferation of idiopathic PAH patients but not that of normal subjects or secondary PAH patients.[28]

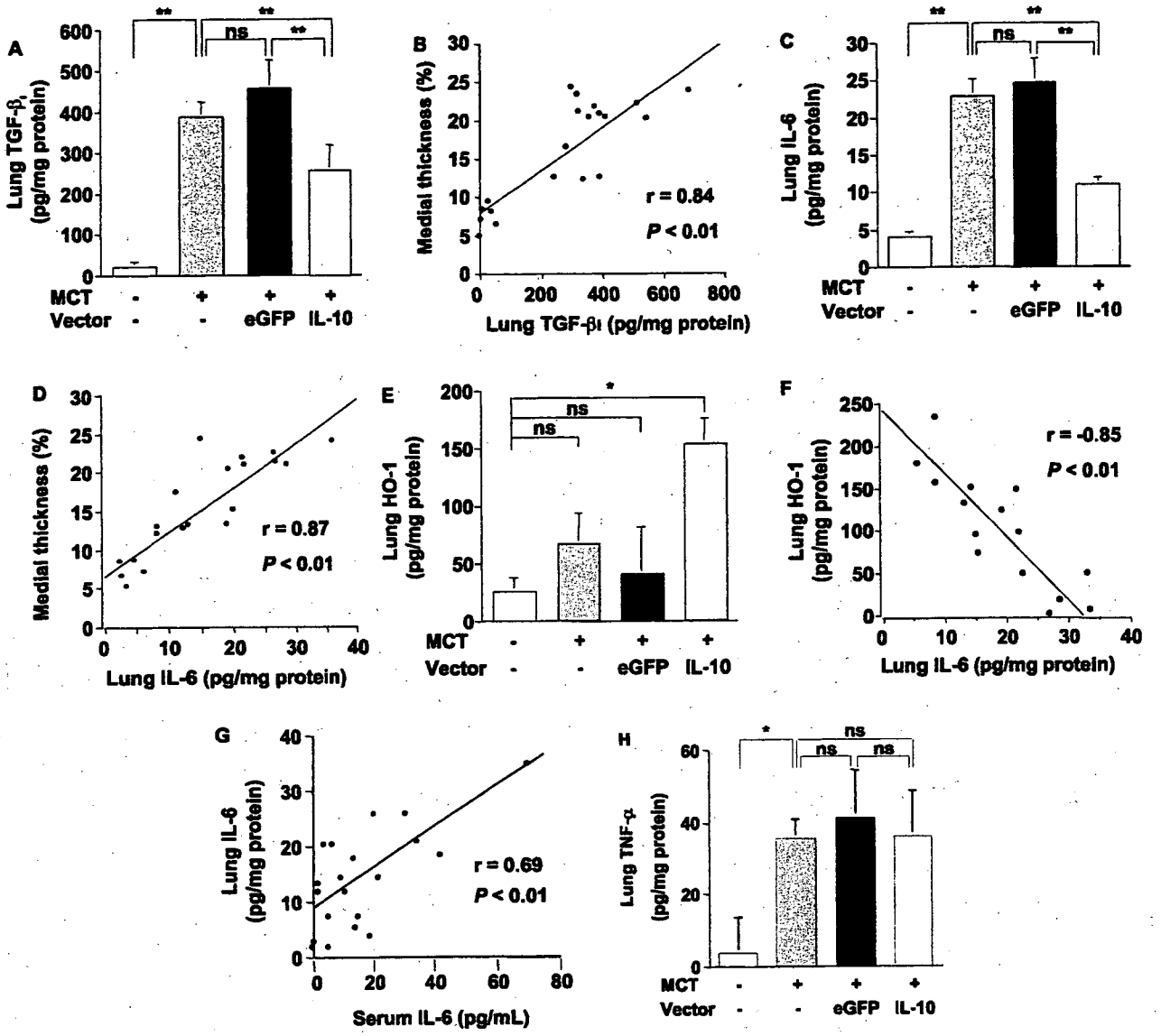

Figure 4. Effects of IL-10 on expression of transforming growth factor-β_1 (TGF-β_1), IL-6, heme oxygenase-1 (HO-1), and tumor necrosis factor-α (TNF-α) in the lung. The 7-week-old Wistar rats were treated with MCT 4 weeks after vector injection. Concentrations of active TGF-β_1 (A), IL-6 (C), HO-1 (E), and TNF-α (H) in the lung extracts were detected using ELISA 4 weeks after MCT treatment. Data represent mean±SEM (n=5 animals per group; *P<0.05, **P<0.01). ns indicates not statistically significant. Correlation between the percent medial thickness and lung levels of TGF-β_1 (B) or IL-6 (D) in rats (groups: NC, MCT, MCT+eGFP, or MCT+IL-10; n=5 animals per group; r=0.84, P<0.01 and r=0.87, P<0.01, respectively). Correlation between the HO-1 and IL-6 (F) levels in the rat lung (groups: MCT, MCT+eGFP, or MCT+IL-10; n=5 animals per group; r=−0.85, P<0.01). Correlation between the lung and serum IL-6 levels (G) in rats (groups: NC, MCT, MCT+eGFP, or MCT+IL-10; n=5 animals per group; r=0.69, P<0.01).

Additionally, TGF-β_1 is accumulated in the hypertrophic PA of both human PAH and MCT-PAH[29,30] and exacerbates PA remodeling.[31]

IL-6, a multifunctional proinflammatory cytokine, acts as a strong mitogen to promote VSMC proliferation.[11] Macrophage infiltration is a hallmark of PAH progression, and activated macrophages produce substantial amounts of IL-6 in MCT-PAH rats.[6,32] In this study, IL-10 treatment inhibited perivascular macrophage infiltration and the lung IL-6 expression in vivo but not IL-6-induced PASMC proliferation in vitro. These results suggest that IL-10 may attenuate IL-6 function indirectly through the decreased accumulation of perivascular macrophages and IL-6. Furthermore, the serum IL-6 levels significantly correlated with the lung IL-6 levels. Because serum IL-6 level reflects the disease activity of idiopathic PAH, it can be a useful biomarker of antiinflammation therapy of PAH. On the other hand, IL-10 did not affect the MCT-induced TNF-α expression in the lung. However, previous studies demonstrated that IL-10 prevents TNF-α–induced VSMC proliferation in vitro.[27] These observations suggest that IL-10 might modulate the downstream signal of TNF-α but not its expression in the setting of MCT-PAH. Overall, IL-10 affects the dynamics of cytokine networks involved in PA remodeling, and its site of action may differ according to the cytokine signal.

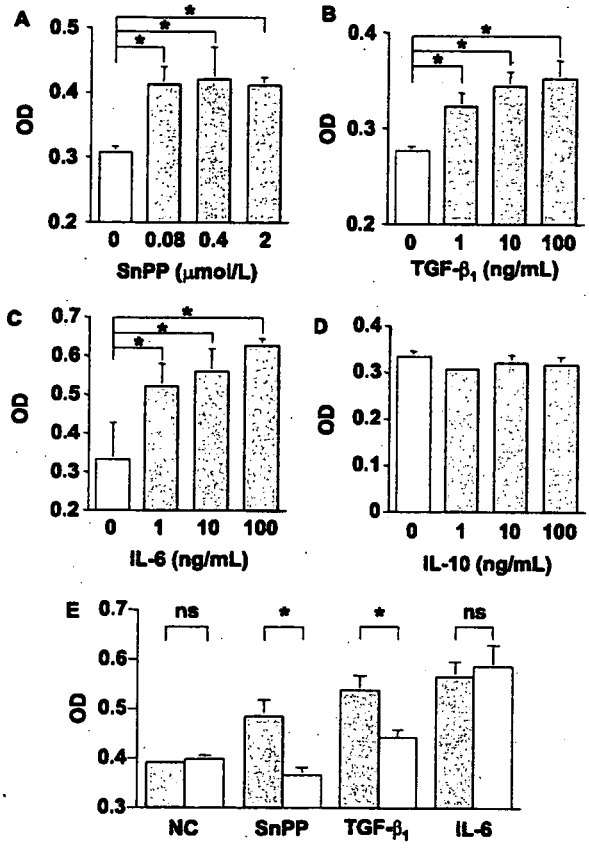

Figure 5. Antiproliferative effects of IL-10 on pulmonary arterial smooth muscle cells (PASMCs). The number of viable human PASMCs cultured in serum-free DMEM-F12 was estimated using a colorimetric assay (XTT assay). The optical density (OD) between 450 nm and 650 nm indicates the extent of cell proliferation. Addition of tin protoporphyrin IX (SnPP, A), TGF-β_1 (B), or IL-6 (C) dose-dependently promotes PASMC proliferation. Although IL-10 alone has no significant effect (D), pretreatment with IL-10 (10 ng/mL) inhibits PASMC proliferation induced by SnPP (2 μmol/L) or TGF-β_1 (20 ng/mL, E) but not that induced by IL-6 (20 ng/mL). Closed columns, cells not treated with IL-10; open columns, IL-10–treated cells. The results are representative of 3 independent experiments. Data represent mean±SEM (n=4 each, *$P<0.05$). ns indicates not statistically significant.

CO induced by HO-1 blocks PASMC proliferation not only directly by inhibiting the expression of a cell cycle–specific transcription factor but also indirectly by attenuating mitogen signaling.[16] Interestingly, the transgenic mice that constitutively express HO-1 are protected from the development of hypoxia-induced PAH and excessive expression of a mitogen IL-6.[33] In this study, AAV-IL-10 administration increased the HO-1 level that negatively correlated with the IL-6 level in the lung of MCT-PAH rats. These observations suggest a dynamic relationship between IL-6 and HO-1 in PA remodeling progression. Chen et al[12] reported that AAV-IL-10 injection enhanced the activity and protein levels of HO-1, but SnPP treatment that inactivates HO-1 reversed the vasculoprotective effects of IL-10 in vivo. Here, we show that pretreatment with recombinant IL-10 suppressed the excessive PASMC proliferation induced by HO-1 inactivation with SnPP. Thus, IL-10 may sustain CO levels by maintaining

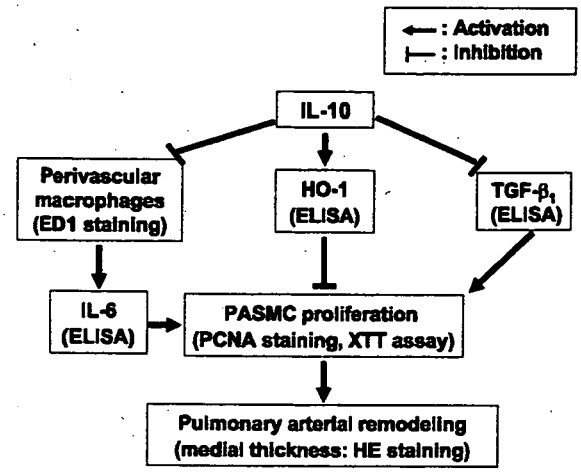

Figure 6. Proposed explanation for IL-10–mediated prevention of PAH and vascular remodeling. Monocrotaline treatment causes PAH in rats by inducing inflammation and proliferation of the PA. IL-10 prevents the development of PAH and PA remodeling by inhibiting vascular inflammation and proliferation. The effects of IL-10 are related to the decreased accumulation of perivascular macrophages and the reduced levels of active TGF-β_1 and IL-6. IL-10 induces HO-1 expression, which can negatively regulate inflammation and proliferation in the PA. IL-10 inhibits abnormal proliferation of PASMCs, thereby preventing PAH development.

HO-1 from inactivating, leading to the prevention of PA remodeling.

Finally, we will discuss the clinical implication and limitations of this study. Consistent with previous studies, maximum gene expression was noted 6 to 8 weeks after the intramuscular injection of AAV vectors. In this study, AAV-IL-10 was injected 4 weeks before MCT administration for the transgene expression to reach plateau levels when MCT-PAH was fully developed (3 to 4 weeks after the injection). Thus, our results are completely based on a prevention protocol, which may be rare in a clinical setting. Intramuscular AAV-IL-10 injection is an attractive candidate for antiinflammation therapy of PAH because inflammatory cytokine expression is associated with the clinical course of the disease. In addition, this strategy exhibited no life-threatening complications such as shock and sepsis which may occur in intravenous prostacyclin infusion therapy. However, therapeutic effects of IL-10 in established PAH has not been determined. Therefore, it should be further examined in studies using a treatment protocol. MCT-PAH is a widely-used and suitable model for exploring inflammatory mechanisms in PAH progression. However, how IL-10 affects other pathogenesis in PAH remains unknown. In the future, IL-10 function needs to be examined in other PAH models such as hypoxia-induced PAH.

In conclusion, AAV vector-mediated sustained IL-10 expression prevented the development of MCT-PAH in rats. The antiremodeling effects of IL-10 are related to the reduction of macrophage infiltration and pathological cytokine expression as well as increased HO-1 levels in the lung. Although the therapeutic role of IL-10 should be further investigated, our results provide new insights into molecular mechanisms underlying the development of human PAH.

Acknowledgments

We thank Miyoko Mitsu for her encouragement and technical support.

Sources of Funding

This work was supported by grants from (1) the Ministry of Health, Labor and Welfare of Japan; (2) Grants-in-Aid for Scientific Research; (3) grant for 21 Century COE Program; (4) "High-Tech Research Center" Project for Private Universities, matching fund subsidy, from the Ministry of Education, Culture, Sports, Science and Technology of Japan; and (5) The Research Award to Jichi Medical School Graduate Student.

Disclosures

None.

References

1. Humbert M, Sitbon O, Simonneau G. Treatment of pulmonary arterial hypertension. *N Engl J Med.* 2004;351:1425–1436.
2. Stenmark KR, Fagan KA, Frid MG. Hypoxia-induced pulmonary vascular remodeling: cellular and molecular mechanisms. *Circ Res.* 2006; 99:675–691.
3. Tuder RM, Groves B, Badesch DB, Voelkel NF. Exuberant endothelial cell growth and elements of inflammation are present in plexiform lesions of pulmonary hypertension. *Am J Pathol.* 1994;144:275–285.
4. Humbert M, Monti G, Brenot F, Sitbon O, Portier A, Grangeot-Keros L, Duroux P, Galanaud P, Simonneau G, Emilie D. Increased interleukin-1 and interleukin-6 serum concentrations in severe primary pulmonary hypertension. *Am J Respir Crit Care Med.* 1995;151:1628–1631.
5. Miyata M, Sakuma F, Yoshimura A, Ishikawa H, Nishimaki T, Kasukawa R. Pulmonary hypertension in rats. 2. Role of interleukin-6. *Int Arch Allergy Immunol.* 1995;108:287–291.
6. Miyata M, Sakuma F, Yoshimura A, Ishikawa H, Nishimaki T, Kasukawa R. Pulmonary hypertension in rats. 1. Role of bromodeoxyuridine-positive mononuclear cells and alveolar macrophages. *Int Arch Allergy Immunol.* 1995;108:281–286.
7. Arcot SS, Lipke DW, Gillespie MN, Olson JW. Alterations of growth factor transcripts in rat lungs during development of monocrotaline-induced pulmonary hypertension. *Biochem Pharmacol.* 1993;46: 1086–1091.
8. Karmochkine M, Wechsler B, Godeau P, Brenot F, Jagot JL, Simonneau G. Improvement of severe pulmonary hypertension in a patient with SLE. *Ann Rheum Dis.* 1996;55:561–562.
9. Bellotto F, Chiavacci P, Laveder F, Angelini A, Thiene G, Marcolongo R. Effective immunosuppressive therapy in a patient with primary pulmonary hypertension. *Thorax.* 1999;54:372–374.
10. Ito T, Ozawa K, Shimada K. Current drug targets and future therapy of pulmonary arterial hypertension. *Curr Med Chem.* 2007;14:719–733.
11. Ito T, Ikeda U. Inflammatory cytokines and cardiovascular disease. *Curr Drug Targets Inflamm Allergy.* 2003;2:257–265.
12. Chen S, Kapturczak MH, Wasserfall C, Glushakova OY, Campbell-Thompson M, Deshane JS, Joseph R, Cruz PE, Hauswirth WW, Madsen KM, Croker BP, Berns KI, Atkinson MA, Flotte TR, Tisher CC, Agarwal A. Interleukin 10 attenuates neointimal proliferation and inflammation in aortic allografts by a heme oxygenase-dependent pathway. *Proc Natl Acad Sci U S A.* 2005;102:7251–7256.
13. Mazighi M, Pelle A, Gonzalez W, Mtairag el M, Philippe M, Henin D, Michel JB, Feldman LJ. IL-10 inhibits vascular smooth muscle cell activation *in vitro* and *in vivo*. *Am J Physiol Heart Circ Physiol.* 2004; 287:H866–H871.
14. Yoshioka T, Okada T, Maeda Y, Ikeda U, Shimpo M, Nomoto T, Takeuchi K, Nonaka-Sarukawa M, Ito T, Takahashi M, Matsushita T, Mizukami H, Hanazono Y, Kume A, Ookawara S, Kawano M, Ishibashi S, Shimada K, Ozawa K. Adeno-associated virus vector-mediated interleukin-10 gene transfer inhibits atherosclerosis in apolipoprotein E-deficient mice. *Gene Ther.* 2004;11:1772–1779.
15. Li MC, He SH. IL-10 and its related cytokines for treatment of inflammatory bowel disease. *World J Gastroenterol.* 2004;10:620–625.
16. Morita T, Mitsialis SA, Koike H, Liu Y, Kourembanas S. Carbon monoxide controls the proliferation of hypoxic vascular smooth muscle cells. *J Biol Chem.* 1997;272:32804–32809.
17. Christou H, Morita T, Hsieh CM, Koike H, Arkonac B, Perrella MA, Kourembanas S. Prevention of hypoxia-induced pulmonary hypertension by enhancement of endogenous heme oxygenase-1 in the rat. *Circ Res.* 2000;86:1224–1229.
18. Yun S, Junbao D, Limin G, Chaomei Z, Xiuying T, Chaoshu T. The regulating effect of heme oxygenase/carbon monoxide on hypoxic pulmonary vascular structural remodeling. *Biochem Biophys Res Commun.* 2003;306:523–529.
19. Matsushita T, Elliger S, Elliger C, Podsakoff G, Villarreal L, Kurtzman GJ, Iwaki Y, Colosi P. Adeno-associated virus vectors can be efficiently produced without helper virus. *Gene Ther.* 1998;5:938–945.
20. Okada T, Nomoto T, Yoshioka T, Nonaka-Sarukawa M, Ito T, Ogura T, Iwata-Okada M, Uchibori R, Shimazaki K, Mizukami H, Kume A, Ozawa K. Large-scale production of recombinant viruses by use of a large culture vessel with active gassing. *Hum Gene Ther.* 2005;16:1212–1218.
21. Okada T, Nomoto T, Shimazaki K, Lijun W, Lu Y, Matsushita T, Mizukami H, Urabe M, Hanazono Y, Kume A, Muramatsu S, Nakano I, Ozawa K. Adeno-associated virus vectors for gene transfer to the brain. *Methods.* 2002;28:237–247.
22. Kay JM, Keane PM, Suyama KL, Gauthier D. Angiotensin converting enzyme activity and evolution of pulmonary vascular disease in rats with monocrotaline pulmonary hypertension. *Thorax.* 1982;37:88–96.
23. Yoshioka T, Ageyama N, Shibata H, Yasu T, Misawa Y, Takeuchi K, Matsui K, Yamamoto K, Terao K, Shimada K, Ikeda U, Ozawa K, Hanazono Y. Repair of infarcted myocardium mediated by transplanted bone marrow-derived $CD34^+$ stem cells in a nonhuman primate model. *Stem Cells.* 2005;23:355–364.
24. Lee TS, Chau LY. Heme oxygenase-1 mediates the anti-inflammatory effect of interleukin-10 in mice. *Nat Med.* 2002;8:240–246.
25. Voelkel NF, Tuder RM, Bridges J, Arend WP. Interleukin-1 receptor antagonist treatment reduces pulmonary hypertension generated in rats by monocrotaline. *Am J Respir Cell Mol Biol.* 1994;11:664–675.
26. Kimura H, Kasahara Y, Kurosu K, Sugito K, Takiguchi Y, Terai M, Mikata A, Natsume M, Mukaida N, Matsushima K, Kuriyama T. Alleviation of monocrotaline-induced pulmonary hypertension by antibodies to monocyte chemotactic and activating factor/monocyte chemoattractant protein-1. *Lab Invest.* 1998;78:571–581.
27. Selzman CH, McIntyre RC Jr, Shames BD, Whitehill TA, Banerjee A, Harken AH. Interleukin-10 inhibits human vascular smooth muscle proliferation. *J Mol Cell Cardiol.* 1998;30:889–896.
28. Morrell NW, Yang X, Upton PD, Jourdan KB, Morgan N, Sheares KK, Trembath RC. Altered growth responses of pulmonary artery smooth muscle cells from patients with primary pulmonary hypertension to transforming growth factor-β_1 and bone morphogenetic proteins. *Circulation.* 2001;104:790–795.
29. Botney MD, Bahadori L, Gold LI. Vascular remodeling in primary pulmonary hypertension. Potential role for transforming growth factor-β. *Am J Pathol.* 1994;144:286–295.
30. Tanaka Y, Schuster DP, Davis EC, Patterson GA, Botney MD. The role of vascular injury and hemodynamics in rat pulmonary artery remodeling. *J Clin Invest.* 1996;98:434–442.
31. El-Haroun H, Bradbury D, Clayton A, Knox AJ. Interleukin-1β, transforming growth factor-β_1, and bradykinin attenuate cyclic AMP production by human pulmonary artery smooth muscle cells in response to prostacyclin analogues and prostaglandin E2 by cyclooxygenase-2 induction and downregulation of adenylyl cyclase isoforms 1, 2, and 4. *Circ Res.* 2004;94:353–361.
32. Suzuki C, Takahashi M, Morimoto H, Izawa A, Ise H, Hongo M, Hoshikawa Y, Ito T, Miyashita H, Kobayashi E, Shimada K, Ikeda U. Mycophenolate mofetil attenuates pulmonary arterial hypertension in rats. *Biochem Biophys Res Commun.* 2006;349:781–788.
33. Minamino T, Christou H, Hsieh CM, Liu Y, Dhawan V, Abraham NG, Perrella MA, Mitsialis SA, Kourembanas S. Targeted expression of heme oxygenase-1 prevents the pulmonary inflammatory and vascular responses to hypoxia. *Proc Natl Acad Sci U S A.* 2001;98:8798–8803.

Adenoassociated Virus–Mediated Prostacyclin Synthase Expression Prevents Pulmonary Arterial Hypertension in Rats

Takayuki Ito, Takashi Okada, Jun Mimuro, Hiroshi Miyashita, Ryosuke Uchibori, Masashi Urabe, Hiroaki Mizukami, Akihiro Kume, Masafumi Takahashi, Uichi Ikeda, Yoichi Sakata, Kazuyuki Shimada, Keiya Ozawa

Adenoassociated Virus–Mediated Prostacyclin Synthase Expression Prevents Pulmonary Arterial Hypertension in Rats

Takayuki Ito, Takashi Okada, Jun Mimuro, Hiroshi Miyashita, Ryosuke Uchibori, Masashi Urabe, Hiroaki Mizukami, Akihiro Kume, Masafumi Takahashi, Uichi Ikeda, Yoichi Sakata, Kazuyuki Shimada, Keiya Ozawa

Abstract—Prostacyclin synthase (PGIS) is the final committed enzyme in the metabolic pathway of prostacyclin production. The therapeutic option of intravenous prostacyclin infusion in patients with pulmonary arterial hypertension is limited by the short half-life of the drug and life-threatening catheter-related complications. To develop a better delivery system for prostacyclin, we examined the feasibility of intramuscular injection of an adenoassociated virus (AAV) vector expressing PGIS for preventing monocrotaline-induced pulmonary arterial hypertension in rats. We developed an AAV serotype 1–based vector carrying a human PGIS gene (AAV-PGIS). AAV-PGIS or the control AAV vector expressing enhanced green fluorescent protein was injected into the anterior tibial muscles of 3-week–old male Wistar rats; this was followed by the monocrotaline administration at 7 weeks. Eight weeks after injecting the vector, the plasma levels of 6-keto-prostaglandin $F_{1\alpha}$ increased in a vector dose-dependent manner. At this time point, the PGIS transduction (1×10^{10} genome copies per body) significantly decreased mean pulmonary arterial pressure (33.9±2.4 versus 46.1±3.0 mm Hg; $P<0.05$), pulmonary vascular resistance (0.26±0.03 versus 0.41±0.03 mm Hg · mL^{-1} · min^{-1} · kg^{-1}; $P<0.05$), and medial thickness of the peripheral pulmonary artery (14.6±1.5% versus 23.5±0.5%; $P<0.01$) as compared with the controls. Furthermore, the PGIS-transduced rats demonstrated significantly improved survival rates as compared with the controls (100% versus 50%; $P<0.05$) at 8 weeks postmonocrotaline administration. An intramuscular injection of AAV-PGIS prevents monocrotaline-pulmonary arterial hypertension in rats and provides a new therapeutic alternative for preventing pulmonary arterial hypertension in humans. (***Hypertension.* 2007;50:531-536.**)

Key Words: hypertension ■ pulmonary ■ gene therapy ■ remodeling ■ prostacyclin synthase

Pulmonary arterial hypertension (PAH) is an intractable disease that leads to increased pulmonary arterial pressure, progressive right heart failure, and premature death; however, no satisfactory treatment has been established for PAH.[1] Although intravenous prostacyclin (PGI_2) therapy prolongs survival in patients with PAH, the use of this treatment option is limited by the short half-life of the drug, requirement for a continuous infusion system, and catheter-related complications.[1,2] PGI_2 synthase (PGIS) is the final committed enzyme in the metabolic pathway of PGI_2 production. PGIS gene transfer is a promising approach for the stable production of endogenous PGI_2.[3–6] However, previous strategies have several limitations both in the selection of delivery routes and in the efficiency of gene expression. For instance, intratracheal gene transfer may deteriorate respiratory function in critically ill subjects, and the intrahepatic approach may cause peritonitis as a result of direct liver puncture. Although an intramuscular approach seems to be safer than the previous approaches, the conventional plasmid-based strategies achieved only transient gene expression and required repeated gene transfer to inhibit pathological remodeling of the pulmonary artery (PA).[6]

In this study, we used an adenoassociated virus (AAV) vector together with an intramuscular approach to obtain more efficient PGI_2 expression. AAV vectors permit efficient and sustained gene expression in nondividing skeletal muscle cells with minimal inflammatory and immune responses. We reported previously that a stable serum concentration of a secretory protein was achieved over a 1-year period by using a single intramuscular injection of several AAV vector (AAV2 and AAV5) serotypes in mice.[7] Currently, AAV1 is one of the most efficient serotypes for muscle transduction.[8,9]

Received March 25, 2007; first decision April 13, 2007; revision accepted June 22, 2007.

From the Divisions of Genetic Therapeutics (T.I., R.U., M.U., H.M., A.K., K.O.), Cardiovascular Medicine (T.I., H.M., K.S.), and Cell and Molecular Medicine (J.M., Y.S.), Jichi Medical University, Tochigi, Japan; the Department of Molecular Therapy (T.O.), National Institute of Neuroscience, National Center of Neurology and Psychiatry, Tokyo, Japan; and the Department of Organ Regeneration (M.T., U.I.), Shinshu University Graduate School of Medicine, Matsumoto, Japan.

Correspondence to Takayuki Ito or Keiya Ozawa, Division of Genetic Therapeutics, Jichi Medical University, 3311-1 Yakushiji, Shimotsuke, Tochigi 329-0498, Japan. E-mail titou@jichi.ac.jp or kozawa@jichi.ac.jp

Hypertension is available at http://hyper.ahajournals.org DOI: 10.1161/HYPERTENSIONAHA.107.091348

Single subcutaneous injection of a pyrrolizidine alkaloid, namely, monocrotaline (MCT), produces severe PAH and PA remodeling in rats. We examined the effects of sustained PGIS expression in preventing PAH development and progression by means of this widely used model and an AAV1 vector.

Methods

Western Blot Analysis for PGIS Expression In Vitro

Human embryonic kidney 293 (HEK293) cells were incubated in 10-cm dishes containing DMEM and nutrient mixture F12 (Invitrogen) with 2% FCS in an atmosphere of 5% CO_2 in air at 37°C. The cells at 70% confluence were transfected with an AAV proviral plasmid encoding human PGIS (phPGIS, a kind gift from Dr Mimuro) or plasmid encoding enhanced green fluorescent protein (eGFP) by using a calcium phosphate method. The cells were harvested 72 hours after transfection, and cell lysates were prepared with a lysis buffer (10 mmol/L of Tris-HCl, 150 mmol/L of NaCl, and 1% NP40 [pH 7.6]) containing Complete Mini protease inhibitor (Roche Diagnostics). For Western blot analysis, 10 μg of the lysate was subjected to 10% SDS-PAGE and transferred to a nitrocellulose membrane. The membrane was blocked and incubated with a 1:500 dilution of rabbit anti-human PGIS polyclonal antibody (a gift from Dr Mimuro) and a 1:5000 dilution of peroxidase-linked anti-rabbit IgG antibody (Amersham Pharmacia Biotech), and immunoreactive bands were visualized using an enhanced chemiluminescence Western blotting kit (Amersham).

AAV-PGIS Production and PGI_2 Expression

We developed a recombinant AAV1-based vector containing the human PGIS or eGFP gene controlled by a modified chicken β-actin promoter with a cytomegalovirus immediate-early enhancer (AAV-PGIS or AAV-eGFP) to obtain efficient transgene expression in skeletal muscle cells. The AAV vectors were prepared according to the previously described 3-plasmid transfection adenovirus-free protocol with minor modifications for enabling the use of an active gassing system.[10,11] In brief, 60% confluent HEK293 cells that were incubated in a large culture vessel with active air circulation were cotransfected with phPGIS, AAV-1 chimeric helper plasmid (p1RepCap), and adenoviral helper plasmid pAdeno (Avigen Inc). The crude viral lysate was purified with 2 rounds of cesium chloride 2-tier centrifugation.[12] The titer of the viral stock was determined against plasmid standards by real-time PCR with primers 5′-CCCGCGAGGTTGTGGTGGAC-3′ and 5′-ATGGGCGGATGCG-GTAGC-3′; subsequently, the stock was dissolved in a buffer (50 mmol/L of HEPES [pH 7.4] and 0.15 mol/L of NaCl [HN buffer]) before infection. The HEK293 cells cultured in 6-well plates containing DMEM and nutrient mixture F12 with 5% FCS were infected with AAV-PGIS at 1×10^4 genome copies per cell to evaluate PGI_2 expression in vitro, and the supernatant was harvested after 72 hours. Concentrations of 6-keto-prostaglandin $F_{1\alpha}$ (6-keto-$PGF_{1\alpha}$) in plasma or culture media were determined by enzyme immunoassay (R&D Systems) according to the manufacturer's instructions. The minimum detectable dose of the assay was <1.4 pg/mL. Interassay and intra-assay precision of the kit was <10%.

Animal Models

All of the animal experiments were approved by the Jichi Medical University ethics committee and were performed in accordance with the National Institutes of Health Guide for the Care and Use of Laboratory Animals. To evaluate the efficiency of gene expression in vivo, AAV-eGFP (200 μL; 1×10^{11} gene copies per body) or AAV-PGIS (200 μL; 1×10^{10} to 1×10^{11} gene copies per body) was injected into the bilateral anterior tibial muscles (n=3 each) of 3-week-old male Wistar rats (Clea Japan Inc) weighing 45 to 55 g. For hemodynamics and histological analyses, the rats were divided into 4 groups: sham rats that were administered the HN buffer (group 1, negative control [NC] group; n=4); MCT-PAH rats administered the HN buffer (group 2, MCT group; n=6); MCT rats administered AAV-eGFP (group 3, MCT+eGFP group; n=6); and MCT rats administered AAV-PGIS (group 4, MCT+PGIS group; n=10). After the anesthesia with spontaneous inhalation of 1% isoflurane, the rats in groups 3 and 4 were intramuscularly injected with AAV-eGFP or AAV-PGIS (1×10^{10} gene copies per body), whereas those in groups 1 and 2 were injected with the HN buffer (200 μL). MCT (Wako Pure Chemicals) was dissolved in 0.1 N HCl, and the pH was adjusted to 7.4 with 1.0 N NaOH. After the anesthesia with spontaneous inhalation of 1% isoflurane, all of the rats except for those in the NC group were injected subcutaneously with MCT (40 mg/kg) 4 weeks after the injecting the vector. Blood samples were collected from the tail vein on ethylenediamine tetraacetic acid tubes, and the concentrations of the leukocytes, platelets, hematocrit, alanine aminotransferase, and creatinine were determined by standard procedures.

Hemodynamics Analysis

Four weeks after the MCT injection, the rats were anesthetized with spontaneous inhalation of 1% isoflurane, and a tracheotomy was performed. Then, they were mechanically ventilated with 1% isoflurane (tidal volume, 10 mL/kg; respiratory rate, 30 breaths per minute) through a tracheostomy. After the thoracic cavity was opened using a midsternal approach, 2F high-fidelity manometer-tipped catheters (SPC-320; Millar Instruments Inc) were inserted directly into the right or left ventricle, and an ultrasonic flow probe (flow probe 2.5S176; Transonic Systems Inc) was placed on the ascending root of the aorta. The heart rate, mean pulmonary arterial pressure (mPAP), aortic systolic arterial pressure, left ventricular end-diastolic pressure (LVEDP), and mean aortic flow indicating the cardiac output (CO) were measured. Cardiac indices (CI) and pulmonary vascular resistance (PVR) were calculated using the following formula: CI ($mL\cdot min^{-1}\cdot kg^{-1}$)=CO/body weight, PVR ($mm\ Hg\cdot mL^{-1}\cdot min^{-1}\cdot kg^{-1}$)=(mPAP−LVEDP)/CI.

Ventricular Weight Measurement and Morphometric Analysis of the PA

After the hemodynamic analysis, the rats were killed with an overdose (5%) of isoflurane through a tracheostomy. Their lungs were perfused with 5 mL of saline followed by 10 mL of cold 4% paraformaldehyde. Each ventricle and the lungs were then excised, dissected free, and weighed. The weight ratio of the right ventricle to the left ventricle plus septum [RV/(LV+S)] was calculated as an index of right ventricular hypertrophy (RVH). The lung tissues were fixed overnight at 4°C in 4% paraformaldehyde and frozen in Tissue-Tek OCT compound (Sakura Finetechnical Co) at −20°C. Hematoxylin and eosin staining was performed on 7-μm–thick sections that were subsequently examined using light microscopy. A morphometric analysis was performed on a PA having an external diameter of 25 to 50 μm or 51 to 100 μm. The medial wall thickness was calculated using the following formula: medial thickness (%)=medial wall thickness/external diameter×100.[13] For the quantitative analysis, 30 vessels of each rat were measured and averaged randomly by the 2 external observers.

Survival Analysis

The 3-week-old Wistar rats were divided into 3 groups (MCT, MCT+eGFP, and MCT+PGIS; n=8 each). After the anesthesia with spontaneous inhalation of 1% isoflurane, the rats in the MCT+eGFP or MCT+PGIS group were intramuscularly injected with AAV-eGFP or AAV-PGIS at 1×10^{10} genome copies per body, respectively. Under the same anesthetic condition, all of the rats were injected subcutaneously with MCT (40 mg/kg) at 4 weeks after injecting the vector. The survival rate was estimated from the date of the MCT administration until death or after 8 weeks of the injection. Survival curves were analyzed using the Kaplan-Meier method and compared by log-rank tests.

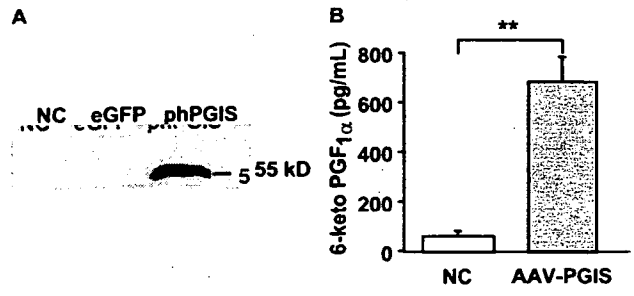

Figure 1. Expression of PGIS and PGI_2 in vitro. A, Western blot analysis of PGIS expression in HEK293 cells after plasmid transfection. The cells were harvested 72 hours after transfection with phPGIS or eGFP. B, AAV vector-mediated PGI_2 expression in HEK293 cells. The PGI_2 levels were estimated by measuring the amount of 6-keto-$PGF_{1\alpha}$, a stable metabolite of PGI_2, in the culture supernatant by enzyme immunoassay 72 hours after infecting the cells (n=4 each) with AAV-PGIS (1×10^4 genome copies per cell). Data are presented as mean±SEM. **$P<0.01$. NC indicates untreated negative control.

Statistical Analysis

The statistical analysis and correlations were performed using StatView (Abacus Concepts, Inc). Data are presented as mean±SEM. Differences in parameters were evaluated using ANOVA combined with Fisher's test. A value of $P<0.05$ was considered statistically significant.

Results

Expression of PGIS and PGI_2 In Vitro

Western blot analysis revealed that transfection of the HEK293 cells with phPGIS but not with a plasmid carrying the eGFP gene enhanced the production of the PGIS protein (Figure 1A). Infection of the cells with AAV-PGIS at 1×10^4 genome copies per cell significantly increased the concentration of 6-keto-$PGF_{1\alpha}$, a stable metabolite of PGI_2, in culture supernatants as compared with that without vector infection (Figure 1B).

AAV Vector-Mediated Systemic PGI_2 Expression in the Rats

Four weeks after the injection of AAV vectors (1×10^{10} genome copies per body), the PGIS-transduced rats began exhibiting significant increases in the plasma 6-keto-$PGF_{1\alpha}$ levels as compared with the control rats (Figure 2A). Eight weeks after the injection, the 6-keto-$PGF_{1\alpha}$ levels increased further in a vector dose-dependent manner in the treated rats (Figure 2B) as compared with the untreated controls (6.68±1.33 versus 1.62±0.30 ng/mL, 1×10^{11} versus 1×10^{10} genome copies per body, respectively; $P<0.05$; n=3 each). The vectors at 1×10^{10} genome copies per body were used for all of the subsequent experiments. In contrast, injection of 1×10^{11} genome copies per body of AAV-eGFP produced no significant change in the 6-keto-$PGF_{1\alpha}$ levels.

Effects of PGI_2 Expression on Hemodynamics and RVH

Four weeks after the MCT administration, the mPAP levels were significantly elevated in the treated rats as compared with the untreated controls (Figure 3A). Treatment with AAV-PGIS but not AAV-eGFP significantly inhibited this increase (Figure 3A). In addition, the expression of PGI_2

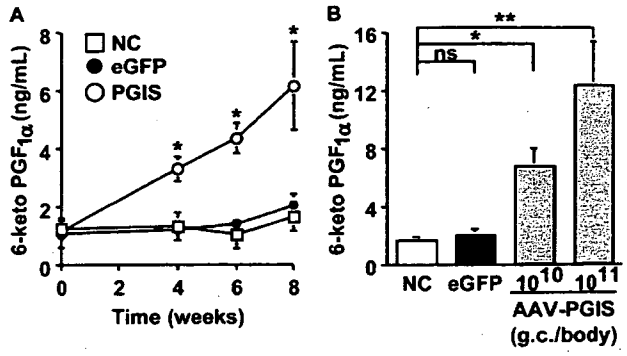

Figure 2. AAV vector-mediated systemic expression of PGI_2 in vivo. The concentration of plasma 6-keto-$PGF_{1\alpha}$ was determined by enzyme immunoassay after a single injection of AAV-PGIS into the anterior tibial muscle of 3-week-old male Wistar rats. A, Time course of plasma 6-keto-$PGF_{1\alpha}$ levels after injection of AAV-PGIS at 1×10^{10} genome copies per body. B, Vector dose dependency of plasma 6-keto-$PGF_{1\alpha}$ levels 8 weeks after the injection. The rats injected with AAV-eGFP (1×10^{11} genome copies per body) were used as controls. Data are presented as mean±SEM (n=3 animals per group). ns indicates not statistically significant; NC, untreated negative control. *$P<0.05$ vs NC; **$P<0.01$.

significantly mitigated an increase in PVR and a decrease in CI that were induced by MCT (Figure 3B and 3C, respectively); however, it produced no significant changes in the heart rate and aortic systolic arterial pressure (Table). PGI_2 expression also had a beneficial effect on RVH. Treatment with AAV-PGIS but not AAV-eGFP significantly inhibited the MCT-induced increase in RV/(LV+S) (Figure 3D).

Effects on Medial Hypertrophy of the PA

Medial hypertrophy is a hallmark of pathological vascular remodeling in PAH. Four weeks after the MCT injection, the

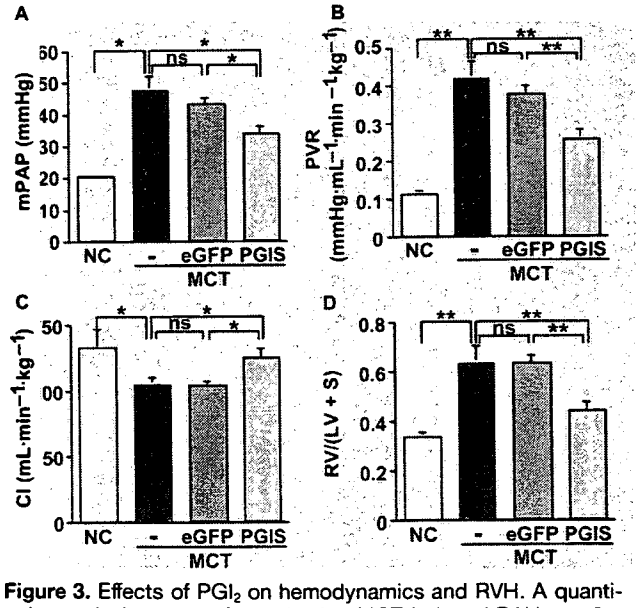

Figure 3. Effects of PGI_2 on hemodynamics and RVH. A quantitative analysis was performed using MCT-induced PAH rats 8 weeks after injecting the vector. A, mPAP (mm Hg); B, PVR (mm Hg · mL^{-1} · min^{-1} · kg^{-1}); C, CI (mL · min^{-1} · kg^{-1}). D, Weight ratio of the right ventricle to the left ventricle plus septum [RV/(LV+S)] presented as an index of RVH. Data are presented as means±SEM (n=4 to 10 animals per group). *$P<0.05$; **$P<0.01$. ns indicates not statistically significant; NC, untreated negative control.

Physiological and Laboratory Data of the MCT-Induced PAH Rats

Factor	NC	MCT	MCT+eGFP	MCT+PGIS	*P*
No. of rats	4	6	6	10	...
Heart rate, per minute	294.0±10.6	281.2±14.7	268.0±9.0	274.8±8.7	NS
ASAP, mm Hg	99.5±1.6	97.3±2.0	96.3±2.4	94.7±4.4	NS
Body weight, g	358.5±11.5	328.3±7.2	328.0±11.4	342.5±9.8	NS
Leukocyte, per mL	6725±372	7917±723	8800±849	8030±852	NS
Hematocrit, %	48.2±0.7	48.9±1.9	51.0±3.0	47.8±1.8	NS
Platelet, $\times 10^4/mm^3$	88.3±8.7	79.2±8.8	80.4±3.6	84.6±6.3	NS
ALT, IU/L	37.8±2.5	49.5±8.4	52.5±6.8	44.1±4.3	NS
Cr, mg/dL	0.52±0.04	0.59±0.05	0.48±0.03	0.53±0.04	NS

Data are presented as means±SEM (n=4 to 10 animals per group). ASAP indicates aortic systolic arterial pressure; ALT, serum alanine aminotransferase; Cr, serum creatinine; NS, not statistically significant.

medial thickness of the PA was greater in the MCT-administered rats than in the untreated controls (Figure 4A). Treatment with AAV-PGIS but not AAV-eGFP prevented the MCT-induced increase in the percentage of medial thickness significantly (Figure 4B, 25 to 50 μm; Figure 4C, 51 to 100 μm in external diameter).

Effects on the Survival of the MCT-PAH Rats and Their Organ Dysfunctions

The PGIS-transduced rats exhibited significantly improved survival rates as compared with the eGFP-transduced rats (Figure 5). The MCT administration produced a slight but not significant decrease in the body weight of the rats, and PGIS gene transfer prevented this decrease. Although the MCT group showed only a slight but not significant increase in the leukocyte count and serum alanine aminotransferase levels as compared with the NC group, the AAV-PGIS treatment caused no additional change in these parameters (Table).

Discussion

The present study demonstrates that sustained PGI_2 expression by a single intramuscular injection of AAV-PGIS prevents the development of MCT-PAH in rats. PGI_2 expression not only increased the cardiac output significantly but also prevented the progression of PVR, RVH, and medial hypertrophy of the PA that was induced by the MCT administration. The PGIS-transduced rats also exhibited significantly improved survival rates as compared with the controls. Furthermore, the PGIS expression observed in this study caused no additional adverse effects on hematologic data and serum indicators of hepatorenal function (alanine aminotransferase and creatinine levels) in the MCT-PAH rats.

The expression of PGI_2 and PGIS decreased in the remodeled PAs of the idiopathic PAH patients.[14,15] Impaired PGI_2 synthesis resulting from a decrease in PGIS expression may be implicated in the pathogenesis of PAH. In fact, continuous intravenous infusion of exogenous PGI_2 markedly lowers PVR and improves survival in PAH patients. However, this system requires lifelong infusion with a central venous catheter because of the short biological half-life of PGI_2. Furthermore, because this system is associated with life-threatening complications (eg, shock and sepsis) that may result in poor survival and quality of life of patients, stable

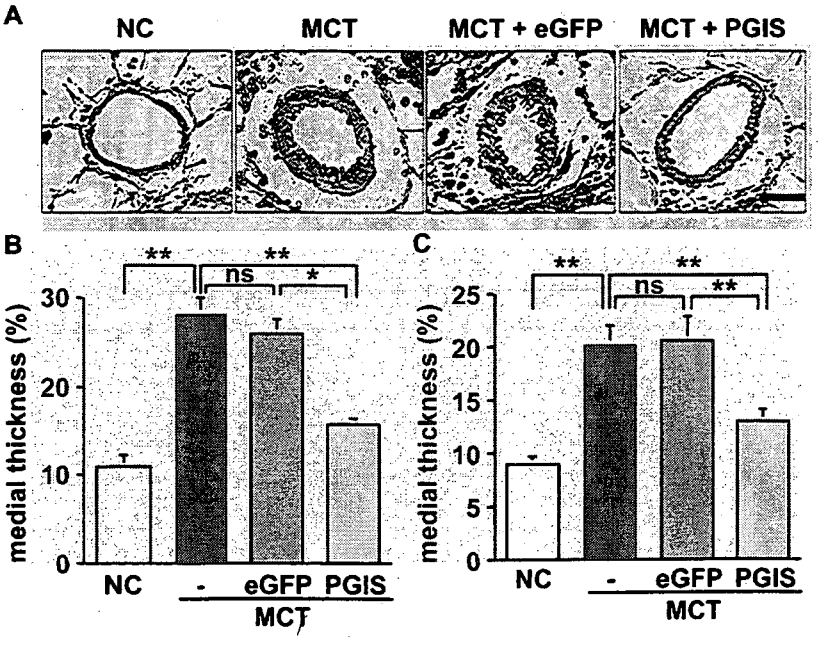

Figure 4. Effects of PGI_2 on medial hypertrophy of the peripheral PA. A, Representative cross-sections of the peripheral PA 4 weeks after the MCT administration (hematoxylin and eosin staining, original magnification, ×1000; scale bar=20 μm). B and C, Quantitative analysis of percentage of medial thickness (B, 25 to 50 μm; C, 51 to 100 μm in external diameter). Data are presented as means±SEM (n=4 to 10 animals per group). *$P<0.05$, **$P<0.01$. ns indicates not statistically significant; NC, untreated negative control.

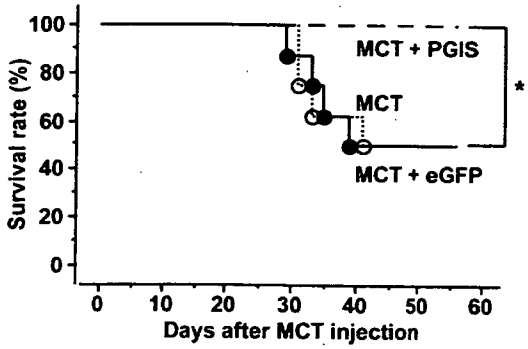

Figure 5. The survival rate of MCT-induced PAH rats. The rats were administered with MCT (40 mg/kg) 4 weeks after the injection of HN buffer (MCT group), AAV-eGFP (MCT+eGFP group), or AAV-PGIS (MCT+PGIS group). The rats were intramuscularly injected with the vectors at 1×10^{10} genome copies per body. The Kaplan-Meier method demonstrated a significant improvement in the survival rate of the rats in the MCT+PGIS group as compared with those in either the MCT or MCT+eGFP group at 8 weeks post-MCT administration. n=8 animals per group; *$P<0.05$ vs MCT or eGFP groups.

production of endogenous PGI_2 would be more desirable. Consistent with previous gene therapy studies, our strategy presented high levels of endogenous PGI_2 expression. In addition, this strategy caused no systemic hypotension and hyperdynamic heart failure, which are the major adverse effects arising from uncontrolled blood levels during intravenous delivery of exogenous PGI_2.[3,4,6]

In this study, we used an AAV serotype 1 vector because it is effective not only in efficient muscle transduction but also in long-term secretion of therapeutic proteins into the systemic circulation. The cDNA for human PGIS shares a high identity with its rat counterpart.[16] In fact, the administration of a plasmid or hemagglutinating virus of the Japan-liposome vector encoding human PGIS successfully ameliorated MCT-PAH. However, the use of these vectors requires repeated administration for achieving sustained gene expression.[3–5] In contrast, the AAV vector used in this study achieved PGIS expression with a single intramuscular injection, and this expression was sustained for 1 year.[7]

Furthermore, gene transfer was believed to be safer when performed via an intramuscular approach as opposed to the intratracheal or intrahepatic approaches.[6] Currently, researchers are using adenoviral gene transfer in most clinical trials because of its high efficiency for gene expression. However, the potential toxic effects of adenoviruses, such as strong immunogenicity, are well known. In contrast, the intramuscular administration of AAV vectors is a promising strategy for delivering therapeutic proteins safely and efficiently, and their use has been examined in clinical trials for hemophilia.[17]

Although PGI_2 is known to be a short-acting vasodilator, recent studies have shown its antiremodeling effects when used in high doses. The administration of PGI_2 analogues cicaprost and iloprost in high concentrations ($>10^{-7}$ mol/L) inhibits mitogen-induced proliferation of rat primary PA smooth muscle cells in a cAMP-dependent manner.[18] Interestingly, another PGI_2 analogue, treprostinil, also inhibits the proliferation of human and mouse primary lung fibroblasts through the activation of a peroxisome proliferator-activated receptor-β/δ when used in equivalent doses.[19] These observations suggest that high levels of PGI_2 may attenuate PA remodeling in vivo through antiproliferative effects. Consistent with previous studies, we demonstrated that high levels of endogenous PGI_2 successfully attenuated medial hypertrophy of the PA.[3,4,6] To discover new drug targets, the roles of peroxisome proliferator-activated receptors and high-level PGI_2 in PAH therapy should be determined, because peroxisome proliferator-activated receptors are associated with many inflammatory and proliferative disorders, including PAH.[2,20]

Finally, we will discuss the clinical implications and limitations of this study. Consistent with previous studies, maximum gene expression was noted 6 to 8 weeks after the intramuscular injection of AAV vectors. AAV-PGIS was injected 4 weeks before MCT administration for the transgene expression to reach plateau levels when MCT-PAH was fully developed (3 to 4 weeks after the injection). Our results are completely based on a preventive protocol, which may be rare in a clinical setting. However, PGI_2 is an established therapeutic molecule, and the advantage of early initiation of PGI_2 therapy for improving survival in patients with idiopathic PAH has been demonstrated in a large clinical trial.[21] These observations convinced us to propose the possible preemptive use of AAV-PGIS as a strategy to maintain basal levels of PGI_2 in patients with mild symptoms of PAH or in those identified as high-risk subjects who have not experienced PAH. As an alternative, the combined use of AAV-PGIS and an initial infusion of intravenous PGI_2 might be promising; the intravenous infusion should be tapered when sufficient levels of PGI_2 are attained. To evaluate the efficacy of AAV-PGIS in a therapeutic protocol (ie, vector injection after the development of PAH), use of a chronic hypoxic PAH model or newly developed self-complementary AAV vectors that can express transgenes earlier than the conventional vectors should be considered.[22]

Perspectives

The present study has demonstrated that the single intramuscular injection of AAV-PGIS achieved a sustained expression of PGI_2. This expression retarded the progression of MCT-PAH in rats without causing significant adverse effects. Thus, this strategy provides a new therapeutic alternative for PAH patients. However, the system in this study lacks the ability to regulate excessive transgene expression. Therefore, regulatory mechanisms to ensure adequate gene expression should be established to facilitate successful translation of this strategy in a clinical setting.

Acknowledgment

We thank Miyoko Mitsu for her encouragement and technical support.

Sources of Funding

This work was supported in part by grants from the Ministry of Health, Labor and Welfare of Japan; Grants-in-Aid for Scientific Research; grant for the 21st Century Centes of Excellence Program; "High-Tech Research Center" Project for Private Universities, matching fund subsidy, from the Ministry of Education, Culture,

Sports, Science and Technology of Japan; and the Research Award to Jichi Medical School Graduate Student.

Disclosures

None.

References

1. Humbert M, Sitbon O, Simonneau G. Treatment of pulmonary arterial hypertension. *N Engl J Med.* 2004;351:1425–1436.
2. Ito T, Ozawa K, Shimada K. Current drug targets and future therapy of pulmonary arterial hypertension. *Curr Med Chem.* 2007;14:719–733.
3. Nagaya N, Yokoyama C, Kyotani S, Shimonishi M, Morishita R, Uematsu M, Nishikimi T, Nakanishi N, Ogihara T, Yamagishi M, Miyatake K, Kaneda Y, Tanabe T. Gene transfer of human prostacyclin synthase ameliorates monocrotaline-induced pulmonary hypertension in rats. *Circulation.* 2000;102:2005–2010.
4. Suhara H, Sawa Y, Fukushima N, Kagisaki K, Yokoyama C, Tanabe T, Ohtake S, Matsuda H. Gene transfer of human prostacyclin synthase into the liver is effective for the treatment of pulmonary hypertension in rats. *J Thorac Cardiovasc Surg.* 2002;123:855–861.
5. Ono M, Sawa Y, Mizuno S, Fukushima N, Ichikawa H, Bessho K, Nakamura T, Matsuda H. Hepatocyte growth factor suppresses vascular medial hyperplasia and matrix accumulation in advanced pulmonary hypertension of rats. *Circulation.* 2004;110:2896–2902.
6. Tahara N, Kai H, Niiyama H, Mori T, Sugi Y, Takayama N, Yasukawa H, Numaguchi Y, Matsui H, Okumura K, Imaizumi T. Repeated gene transfer of naked prostacyclin synthase plasmid into skeletal muscles attenuates monocrotaline-induced pulmonary hypertension and prolongs survival in rats. *Hum Gene Ther.* 2004;15:1270–1278.
7. Yoshioka T, Okada T, Maeda Y, Ikeda U, Shimpo M, Nomoto T, Takeuchi K, Nonaka-Sarukawa M, Ito T, Takahashi M, Matsushita T, Mizukami H, Hanazono Y, Kume A, Ookawara S, Kawano M, Ishibashi S, Shimada K, Ozawa K. Adeno-associated virus vector-mediated interleukin-10 gene transfer inhibits atherosclerosis in apolipoprotein E-deficient mice. *Gene Ther.* 2004;11:1772–1779.
8. Chen S, Kapturczak MH, Wasserfall C, Glushakova OY, Campbell-Thompson M, Deshane JS, Joseph R, Cruz PE, Hauswirth WW, Madsen KM, Croker BP, Berns KI, Atkinson MA, Flotte TR, Tisher CC, Agarwal A. Interleukin 10 attenuates neointimal proliferation and inflammation in aortic allografts by a heme oxygenase-dependent pathway. *Proc Natl Acad Sci U S A.* 2005;102:7251–7256.
9. Mu W, Ouyang X, Agarwal A, Zhang L, Long DA, Cruz PE, Roncal CA, Glushakova OY, Chiodo VA, Atkinson MA, Hauswirth WW, Flotte TR, Rodriguez-Iturbe B, Johnson RJ. IL-10 suppresses chemokines, inflammation, and fibrosis in a model of chronic renal disease. *J Am Soc Nephrol.* 2005;16:3651–3660.
10. Matsushita T, Elliger S, Elliger C, Podsakoff G, Villarreal L, Kurtzman GJ, Iwaki Y, Colosi P. Adeno-associated virus vectors can be efficiently produced without helper virus. *Gene Ther.* 1998;5:938–945.
11. Okada T, Nomoto T, Yoshioka T, Nonaka-Sarukawa M, Ito T, Ogura T, Iwata-Okada M, Uchibori R, Shimazaki K, Mizukami H, Kume A, Ozawa K. Large-scale production of recombinant viruses by use of a large culture vessel with active gassing. *Hum Gene Ther.* 2005;16:1212–1218.
12. Okada T, Nomoto T, Shimazaki K, Lijun W, Lu Y, Matsushita T, Mizukami H, Urabe M, Hanazono Y, Kume A, Muramatsu S, Nakano I, Ozawa K. Adeno-associated virus vectors for gene transfer to the brain. *Methods.* 2002;28:237–247.
13. Kay JM, Keane PM, Suyama KL, Gauthier D. Angiotensin converting enzyme activity and evolution of pulmonary vascular disease in rats with monocrotaline pulmonary hypertension. *Thorax.* 1982;37:88–96.
14. Christman BW, McPherson CD, Newman JH, King GA, Bernard GR, Groves BM, Loyd JE. An imbalance between the excretion of thromboxane and prostacyclin metabolites in pulmonary hypertension. *N Engl J Med.* 1992;327:70–75.
15. Tuder RM, Cool CD, Geraci MW, Wang J, Abman SH, Wright L, Badesch D, Voelkel NF. Prostacyclin synthase expression is decreased in lungs from patients with severe pulmonary hypertension. *Am J Respir Crit Care Med.* 1999;159:1925–1932.
16. Miyata A, Hara S, Yokoyama C, Inoue H, Ullrich V, Tanabe T. Molecular cloning and expression of human prostacyclin synthase. *Biochem Biophys Res Commun.* 1994;200:1728–1734.
17. High K. AAV-mediated gene transfer for hemophilia. *Genet Med.* 2002; 4:56S–61S.
18. Phillips PG, Long L, Wilkins MR, Morrell NW. cAMP phosphodiesterase inhibitors potentiate effects of prostacyclin analogs in hypoxic pulmonary vascular remodeling. *Am J Physiol Lung Cell Mol Physiol.* 2005;288: L103–L115.
19. Ali FY, Egan K, FitzGerald GA, Desvergne B, Wahli W, Bishop-Bailey D, Warner TD, Mitchell JA. Role of prostacyclin versus peroxisome proliferator-activated receptor beta receptors in prostacyclin sensing by lung fibroblasts. *Am J Respir Cell Mol Biol.* 2006;34:242–246.
20. Ameshima S, Golpon H, Cool CD, Chan D, Vandivier RW, Gardai SJ, Wick M, Nemenoff RA, Geraci MW, Voelkel NF. Peroxisome proliferator-activated receptor gamma (PPARgamma) expression is decreased in pulmonary hypertension and affects endothelial cell growth. *Circ Res.* 2003;92:1162–1169.
21. Sitbon O, Humbert M, Nunes H, Parent F, Garcia G, Herve P, Rainisio M, Simonneau G. Long-term intravenous epoprostenol infusion in primary pulmonary hypertension: prognostic factors and survival. *J Am Coll Cardiol.* 2002;40:780–788.
22. Nathwani AC, Gray JT, McIntosh J, Ng CY, Zhou J, Spence Y, Cochrane M, Gray E, Tuddenham EG, Davidoff AM. Safe and efficient transduction of the liver after peripheral vein infusion of self-complementary AAV vector results in stable therapeutic expression of human FIX in nonhuman primates. *Blood.* 2007;109:1414–1421.

EXPERIMENTAL and MOLECULAR MEDICINE, Vol. 39, No. 2, 170-175, April 2007

Promoter effects of adeno-associated viral vector for transgene expression in the cochlea *in vivo*

Yuhe Liu[1,3], Takashi Okada[2], Tatsuya Nomoto[2], Xiaomei Ke[1], Akihiro Kume[2], Keiya Ozawa[2] and Shuifang Xiao[1]

[1]Department of Otolaryngology
Head and Neck Surgery, Peking University First Hospital
Beijing 100034, China
[2]Division of Genetic Therapeutics
Center for Molecular Medicine
Jichi Medical School
Tochigi 329-0498, Japan
[3]Corresponding author: Tel, 86-10-63078547;
Fax, 86-10-66173427; E-mail, liuyuhe@xinhuanet.com

Accepted 6 February 2007

Abbreviations: AAV, adeno-associated virus; CAG, cytomegalovirus IE enhancer and chicken β-actin promoter; CMV, cytomegalovirus promoter; EF-1α, elongation factor 1 alpha promoter; EGFP, enhanced green fluorescent protein; ITRs, inverted terminal repeats; Myo, myosin 7A promoter; NSE, neuron-specific enolase promoter; RSV, Rous sarcoma virus promoter; WPRE, woodchuck hepatitis; virus posttranscriptional regulatory element

Abstract

The aims of this study were to evaluate the expression of enhanced green fluorescent protein (EGFP) driven by 6 different promoters, including cytomegalovirus IE enhancer and chicken β–actin promoter (CAG), cytomegalovirus promoter (CMV), neuron-specific enolase promoter (NSE), myosin 7A promoter (Myo), elongation factor 1α promoter (EF-1α), and Rous sarcoma virus promoter (RSV), and assess the dose response of CAG promoter to transgene expression in the cochlea. Serotype 1 adeno-associated virus (AAV1) vectors with various constructs were transduced into the cochleae, and the level of EGFP expression was examined. We found the highest EGFP expression in the inner hair cells and other cochlear cells when CAG promoter was used. The CMV and NSE promoter drove the higher EGFP expression, but only a marginal activity was observed in EF-1α promoter driven constructs. RSV promoter failed to drive the EGFP expression. Myo promoter driven EGFP was exclusively expressed in the inner hair cells of the cochlea. When driven by CAG promoter, reporter gene expression was detected in inner hair cells at a dose as low as 3×10^7 genome copies, and continued to increase in a dose-dependent manner. Our data showed that individual promoter has different ability to drive reporter gene expression in the cochlear cells. Our results might provide important information with regard to the role of promoters in regulating transgene expression and for the proper design of vectors for gene expression and gene therapy.

Keywords: cochlea; dependovirus; gene therapy; gene transfer techniques; green fluorescent proteins; promoter regions

Introduction

Gene transfer is a promising tool to study the physiology of the cochlea and cochlear cells. The feasibility of gene therapy in the cochlea has been established (Dazert *et al.*, 2001; Kawamoto *et al.*, 2001; Liu *et al.*, 2005), still, there is a controversy about the transduction of the hair cells or spiral ganglion cell, even when the same vehicle is employed as vectors, such as adenovirus and adeno-associated virus (AAV) (Luebke *et al.*, 2001; Li *et al.*, 2002; Yamasoba *et al.*, 2002; Liu *et al.*, 2005). The previous studies support the hypothesis that this discrepancy may be caused by the differences in delivery methods or driven promoters. It has been shown that individual promoter has distinct ability to express reporter genes in different cell types (Chung *et al.*, 2002; Nomoto *et al.*, 2003; Shevtsova *et al.*, 2005). Tissue or cell specific promoters are capable of restricting gene expression in desirable cells and facilitating persistent or regulated transgene expression (Liu *et al.*, 2004). The cytomegalovirus IE enhancer and chicken β-actin promoter (CAG) drives high level of transgene expression and is one of the most commonly used promoters for gene transfer (Xu *et al.*, 2001). The myosin 7A promoter (Myo) was shown to be the specific promoter of hair cells in the cochlea (Boeda *et al.*, 2001). We have previously demonstrated that, with AAV1 vectors, the CAG promoter can drive transgene expression in the cochlea cells at a highly functional level (Liu *et al.*, 2005). In the present study, we systematically evaluated the promoters CAG, Myo, cytomegalovirus

promoter (CMV), elongation factor 1 alpha promoter (EF-1α), neuron-specific enolase promoter (NSE), and rous sarcoma virus promoter (RSV) for their abilities in gene transfers to the cochlear cells using *in vivo* assays. We also examined the dose-response relationship for CAG promoter over a broad range in the cochlea.

Materials and Methods

Construction and preparation of the proviral plasmids

The AAV1 vector proviral plasmid, pAAV2-*LacZ*, harbors an *Escherichia coli* β-galactosidase expression cassette with the CMV promoter, human growth hormone first intron, and SV40 early polyadenylation sequence; flanked by inverted terminal repeats (ITRs) (Okada *et al.*, 2002). The proviral plasmid pAAV2-CAG-EGFP-WPRE (pAAV2-CAG) consists of enhanced green fluorescent protein (EGFP) gene under the control of the CAG promoter and Woodchuck hepatitis virus posttranscriptional regulatory element (WPRE) and is flanked by ITRs (Liu *et al.*, 2005). *Age*I restriction site was created on 5' end of Myo promoter (Boeda *et al.*, 2001) from C2C12 cell line genomic DNA when subcloned into pCRII-TOPO by PCR (forward primer: 5'-ATGTCGACCT-TGGGCAACCTCTAGACG-3'; reverse primer: 5'-ATC-CGCGGCTTCTACGTCTGCACAC-3'). *Spe*I-*Age*I fragment containing the Myo promoter was subcloned into pAAV2-CAG to obtain pAAV2-Myo-EGFP-WPRE (pAAV2-Myo). PAAV2-CMV-EGFP-WPRE (pAAV2-CMV), pAAV2-EF1α-EGFP-WPRE (pAAV2-EF1α), pAAV2-NSE-EGFP-WPRE (pAAV2-NSE), and pAAV2-RSV-EGFP-WPRE (pAAV2-RSV) were constructed as previously described (Ogasawara *et al.*, 1998; Nomoto *et al.*, 2003; Mochizuki *et al.*, 2004). A schematic illustration of the AAV1 vectors is shown in Figure 1. AAV1-helper plasmid harbors Rep and Cap. Adenovirus helper plasmid pAdeno5 identical to pVAE2AE4-5 encodes the entire E2A and E4 regions, and VA RNA I and II genes (Matsushita *et al.*, 1998). Plasmids were purified with the QIAGEN plasmid purification Kits (QIAGEN K.K., Tokyo, Japan).

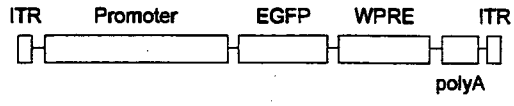

Figure1. Schematic representations of viral vectors constructed. AAV1 vectors were constructed using different promoters to drive reporter gene EGFP and the SV40 polyadenylation sequences (polyA). The promoters in the study include CAG, CMV, NSE, Myo, EF-1α and RSV. The Woodchuck hepatitis virus posttranscriptional regulatory element (WPRE) was inserted 3' of the EGFP cassette in the vectors. ITR, inverted terminal repeats.

Recombinant AAV1 vectors production

Vectors were produced with the AAV1 packaging plasmids pAAV1RepCap and the AAV1 proviral plasmid pAAV2-CAG, pAAV2-Myo, pAAV2-CMV, pAAV2-EF1α, pAAV2-NSE, or pAAV2-RSV. Six kinds of AAV1 vectors were produced using three-plasmid transfection adenovirus-free protocol (Liu *et al.*, 2005). Recombinant AAV1 was harvested at 72 h after transfection by three cycles of freeze/thawing. The crude viral lysate was then purified twice on a cesium chloride (CsCl) two-tier centrifugation gradient as previously described (Okada *et al.*, 2002). The viral stock was titrated by the quantitative real-time PCR of DNase-treated stocks with plasmid standards (Veldwijk *et al.*, 2002). Thus, AAV1 vectors of AAV1-CAG-EGFP-WPRE (AAV1-CAG), AAV1-Myo-EGFP-WPRE (AAV1-Myo), AAV1-CMV-EGFP-WPRE (AAV1-CMV), AAV1-EF1α-EGFP-WPRE (AAV1-EF1α), AAV1-NSE-EGFP-WPRE (AAV1-NSE), and AAV1-RSV-EGFP-WPRE (AAV1-RSV) were constructed. The titers of AAV1 vectors were from 6×10^{12} to 8×10^{13} genome copies (g.c.). For dose-response relationship experiment, vector stocks were serially diluted with artificial perilymph (AP: 145 mM NaCl, 2.7 mM KCl, 2 mM $MgSO_4$, 1.2 mM $CaCl_2$, 5 mM HEPES).

Evaluation of the *in vitro* activity of recombinant AAV1 vectors

To examine the functions of individual promoters, HEK 293 cells were cultured for 36 h, and then transfected with various AAV1 vectors separately (1×10^4 g.c./cell). *Myosin 7A* gene is transcribed in several epithelial cell types that possess microvilli, i.e. renal epithelial cell. Since HEK 293 cell line has been originated from human embryonic kidney epithelial cell, the Myo promoter activity can be assessed in this particular cell line. Forty-eight h after transduction, the cells were recorded for EGFP expression using OLYMPUS IX70 (Olympus corporation, Tokyo, Japan) fluorescence microscope. Cells with green fluorescence were considered "positive" for transgene expression.

Surgical procedures and cochlear perfusions

All animal studies were approved by the ethics committee of Jichi Medical School in Japan and Peking University First Hospital in China. They were performed following the animal research guidelines at Jichi Medical School and Peking University First

Hospital. Seventy female C57BL/6J mice (4 weeks old, CLEA Japan, Tokyo, Japan) and 30 male Sprague-Dawley rats (5 weeks old, CLEA Japan, Tokyo, Japan) with normal Preyer's reflexes were included in this study. Surgical procedures and cochlear perfusion of the animals were performed as previously described (Liu *et al.*, 2005). In the testing groups, 5 μl of AAV1 vectors solution was microinjected into the unilateral cochlea. Five mice received control cochlear perfusions with artificial perilymph only. Each AAV1 vector was injected into 5 animals with 3×10^{10} g.c./cochlea. Injected dose of AAV1-CAG vector into 5 mice was varied from 3×10^{10} to 3×10^{7} g.c./cochlea for dose response study.

Histological study

The capability of the transgene expression in the cochlear cells for various AAV1 vectors was determined by visualizing EGFP levels. The animals were sacrificed 2 weeks after injection, and the cochleae were harvested and the stapes footplates were removed. After fixing and decalcifying, the cochleae were made by cryosection (10 μm). The EGFP expression was detected under OLYMPUS IX70 fluorescence microscope using a standard fluoresce in isothiocyanate (FITC) filter set and a Studio Lite software (Olympus corporation, Tokyo, Japan). Level of expression was graded by fluorescent intensity.

Results

Evaluation of activity of all promoters *in vitro*

The EGFP expression in the HEK 293 cell was detected with any of the AAV1 vectors, indicating that all promoters were functional. However, their expression levels were different (Figure 2). Robust EGFP expression with CAG promoter was shown in the HEK 293 cell, followed by CMV, NSE, EF-1α and RSV. Myo promoter was just weak in 293 cells.

EGFP expression profile within the cochlea under different promoter

The pattern of EGFP expression in the cochlear cells was quite similar in both mice and rat for each promoter. Distribution of AAV1 vector-mediated EGFP expression was examined throughout the cochlea for all promoters tested (Table 1). With CAG promoter, a robust EGFP expression was identified in the various cochlear cells, including the inner hair cells, spiral ganglion cells, inner sulcus cells, Hensen's cells and mesenchymal cells (Figure 3B). A

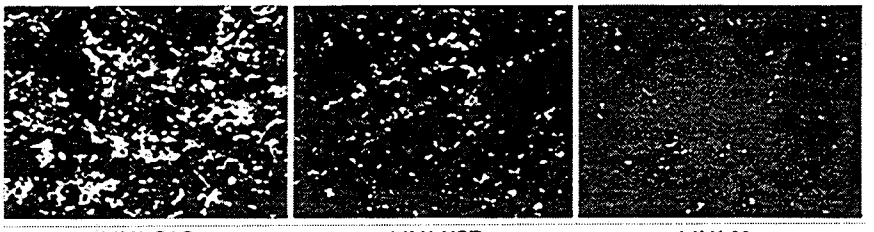

Figure 2. EGFP expression in the HEK293 cell transduced with AAV1 vectors harboring distinct promoters. Robust EGFP expression with CAG promoter was shown, EGFP expression with CMV is similar to that with CAG, and EGFP expression with NSE to with RSV and EF-1α. Myo promoter was just weak in 293 cells.

Table 1. Transgene expression with distinct promoter in the cochlear cells

Promoter	Inner hair cells	Outer hair cells	Spiral ganglion cells	Stria vascularis cells	Spiral ligament cells	Reissner's membrane	Inner sulcus cells	Claudius' cells	Mesenchymal cells
CAG	+	-	+	-	+	+	+	-	+
CMV	+	-	+	-	+	+	+	-	+
NSE	-	-	+	-	+	+	-	-	+
EF-1α	-	-	+	-	+	-	-	-	+
Myo	+	-	-	-	-	-	-	-	-
RSV	-	-	-	-	-	-	-	-	-

+ means EGFP expression in the cells, while - means no fluorescence in the cells.

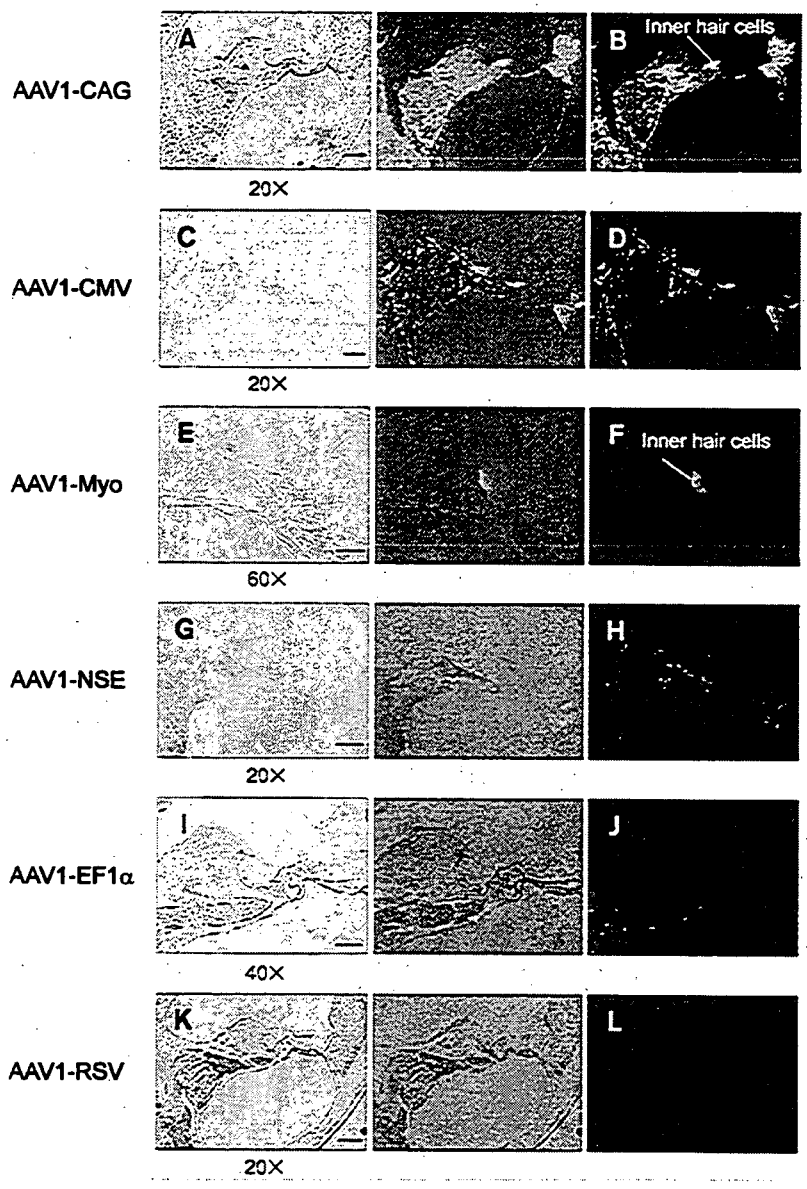

Figure 3. Transduction of cochlear radical cryosection with AAV1 vectors harboring distinct promoters showing EGFP expression in the cochlear various cells. Light photomicrograph of cochlear cryosection is shown in (A,C,E,G,I,K). The fluorescence photomicrograph (green fluorescence from transgene) of the cryosection is shown in (B,D,F,H,J,L). Scale bar, 20×: 50; 40×: 25; 60×: 25 μm separately.

similar transgene expression pattern (Figure 3D) was also observed when AAV1-CMV vector was used. In contrast, the EGFP expression under NSE and EF- 1α promoters was present in all kinds but the inner hair cells of cochlear cells (Figure 3H and J). As reported previously (Boeda *et al.*, 2001), Myo promoter driven EGFP was exclusively expressed in the inner hair cells of cochlea (Figure 3F), while EGFP expression in the cochlear cells was rarely observed with the RSV promoter (Figure 3L). Consistent with the previous findings (Liu *et al.*, 2005), no EGFP expression was detected in the outer hair cells, supporting pillar cells, or the stria vascularis cells with all tested promoters. The level of EGFP expression in the cochlear cells was highest with CAG promoter, followed by CMV promoter. NSE promoter only drove weak expression of EGFP, while EF-1α promoter displayed the least activity.

Our results indicate that, among these promoters, CAG promoter was the most efficient in transducing the cochlear cells.

Dose-response relationship for AAV1-CAG vector

Within the dose-effect groups with AAV1-CAG, a significant effect of dosage on the number of EGFP-expressing cochlear cells was found by one-way ANOVA ($P < 0.001$). CAG promoter driven EGFP expression in inner hair cells was detected at a dose as low as 3×10^7 genome copies, with expression increasing in a dose-dependent manner.

Discussion

The various factors affecting the transcription of a transgene includes the promoter containing 5'flanking region, 3'UTR, enhancer, suppressor, insulator sequences and the type and activity of transcription factors available in the transfected cells. This study showed that all 6 promoters, including viral, mammalian cells promoters, were capable of driving EGFP expression in HEK 293 cells, suggesting that the HEK 293 cell possesses all essential transcription factors for recognizing the diverse promoter sequences applied in this study. The CAG promoter appeared to be more efficient than other promoters based on the following observations: (1) more cells transduced in an equal dose comparison; (2) greater spreads of EGFP-expressing cell groups; and (3) CAG promoter-driven expression in more cell types, especially the inner hair cells, which were rarely found with other promoters except for CMV promoter. These results extend our knowledge about the promoter-related characteristics of AAV1-mediated gene transfer in the cochlea.

Interestingly, our data demonstrate that, in comparison with NSE, EF-1α and RSV promoters, CAG, CMV and hair cells specific promoter-Myo can drive EGFP expression in the inner hair cells. Even though certain promoters, such as EF-1α and RSV promoters, showed robust activity in many tissues, their activities are limited in the cochlear cells. Nowadays, it still has not been known why NSE, EF-1α and RSV promoters are inactive in the inner hair cells. One likely explanation is that inner hair cells may not express some transcription factors, which were necessary for these promoters to be actived. On the other hand, the inner hair cells may have all necessary components for the full transcriptional activity of the CAG, CMV or Myo promoters. Another possibility is transcriptional shutdown or promoter silencing in the inner hair cells. These phenomena have been observed previously in different organs such as the liver, lungs, and muscles (Hartikka *et al.*, 1996; Chen *et al.*, 2001; Gill *et al.*, 2001). Besides the known mechanisms for promoter silencing, such as DNA methylation, it has been demonstrated that the inclusion of EBN1 and OriP sequences into vector constructs may delay the process of promoter silencing (Al-Dosari *et al.*, 2006). Those elements also have been known to play an important role during viral infection in retention, replication, nuclear localization, binding to the nuclear matrix of the target cell, and tran-scriptional up-regulation (Cui *et al.*, 2001). Nevertheless, the mechanism of promoter inactivation remains to be poorly understood. The development of the vectors, which was capable of expressing high levels of transgene products, remains as an occasional finding. A thorough investigation on the mechanisms underlying episomal gene expression would be important for successful development of gene therapy.

Dose-dependent response for AAV gene transfer in other tissue has been previously reported (Klein *et al.*, 2002), and the wide range of doses has established minimal doses for transgene expression (10^7 particles). There is a shift toward lower potency for bicistronic vectors. The present study determined the dose dependency and minimum effective doses for AAV1 gene transfer using CAG promoter for the cochlear cells.

The direct measurement of transgene expression level in individual cells of cochlea *in vivo* is an important evaluation for cochlear gene therapy. Nevertheless, quantifying the number of cells transduced remains an important additional issue and a combination of protein expression and cell transduction efficiency may permit us to estimate the amount of gene product per cell under appropriate conditions. The gene transduction of the cochlear inner hair cells requires efficient promoter systems, which ensure potent and stable expression of exogenous genes. In this study, we demonstrated that the CAG and CMV promoters showed stable and efficient activity in the cochlear cells, the Myo promoter was specific for gene transfer in the inner hair cells. The stable and efficient promoter activities might be necessary for cochlear gene therapy strategies. From the data obtained by this study, it might be able to extend our knowledge both in the basic and clinical gene research fields.

Acknowledgement

This study was supported in part by Research Grants from the Ministry of Education, Culture, Sports, Science and Technology, the Ministry of Health, Labor and Welfare, and the Vehicle Racing Commemorative Foundation.

References

Al-Dosari M, Zhang G, Knapp JE, Liu D. Evaluation of viral and mammalian promoters for driving transgene expression in mouse liver. Biochem Biophys Res Commun 2006;339:673-8

Boeda B, Weil D, Petit C. A specific promoter of the sensory cells of the inner ear defined by transgenesis. Hum Mol Genet 2001;10:1581-9

Chen ZY, Yant SR, He CY, Meuse L, Shen S, Kay MA. Linear DNAs concatemerize *in vivo* and result in sustained transgene expression in mouse liver. Mol Ther 2001;3:403-10

Chung S, Andersson T, Sonntag KC, Bjorklund L, Isacson O, Kim KS. Analysis of different promoter systems for efficient transgene expression in mouse embryonic stem cell lines. Stem Cells 2002;20:139-45

Cui FD, Kishida T, Ohashi S, Asada H, Yasutomi K, Satoh E, Kubo T, Fushiki S, Imanishi J, Mazda O. Highly efficient gene transfer into murine liver achieved by intravenous administration of naked Epstein-Barr virus (EBV)-based plasmid vectors. Gene Ther 2001;8:1508-13

Dazert S, Aletsee C, Brors D, Gravel C, Sendtner M, Ryan A. *In vivo* adenoviral transduction of the neonatal rat cochlea and middle ear. Hear Res 2001;151:30-40

Gill DR, Smyth SE, Goddard CA, Pringle IA, Higgins CF, Colledge WH, Hyde SC. Increased persistence of lung gene expression using plasmids containing the ubiquitin C or elongation factor 1alpha promoter. Gene Ther 2001;8:1539-46

Hartikka J, Sawdey M, Cornefert-Jensen F, Margalith M, Barnhart K, Nolasco M, Vahlsing HL, Meek J, Marquet M, Hobart P, Norman J, Manthorpe M. An improved plasmid DNA expression vector for direct injection into skeletal muscle. Hum Gene Ther 1996;7:1205-17

Kawamoto K, Oh SH, Kanzaki S, Brown N, Raphael Y. The functional and structural outcome of inner ear gene transfer via the vestibular and cochlear fluids in mice. Mol Ther 2001;4:575-85

Klein RL, Hamby ME, Gong Y, Hirko AC, Wang S, Hughes JA, King MA, Meyer EM. Dose and promoter effects of adeno-associated viral vector for green fluorescent protein expression in the rat brain. Exp Neurol 2002;176: 66-74

Li Duan M, Bordet T, Mezzina M, Kahn A, Ulfendahl M. Adenoviral and adeno-associated viral vector mediated gene transfer in the guinea pig cochlea. Neuroreport 2002;13: 1295-9

Liu BH, Wang X, Ma YX, Wang S. CMV enhancer/human PDGF-beta promoter for neuron-specific transgene expression. Gene Ther 2004;11:52-60

Liu Y, Okada T, Sheykholeslami K, Shimazaki K, Nomoto T, Muramatsu SI, Kanazawa T, Takeuchi K, Ajalli R, Mizukami H, Kume A, Ichimura K, Ozawa K. Specific and efficient transduction of cochlear inner hair cells with recombinant adeno-associated virus type 3 vector. Mol Ther 2005;12:725-733

Luebke AE, Foster PK, Muller CD, Peel AL. Cochlear function and transgene expression in the guinea pig cochlea, using adenovirus- and adeno-associated virus-directed gene transfer. Hum Gene Ther 2001;12:773-81

Matsushita T, Elliger S, Elliger C, Podsakoff G, Villarreal L, Kurtzman GJ, Iwaki Y, Colosi P. Adeno-associated virus vectors can be efficiently produced without helper virus. Gene Ther 1998;5:938-45

Mochizuki S, Mizukami H, Kume A, Muramatsu S, Takeuchi K, Matsushita T, Okada T, Kobayashi E, Hoshika A, Ozawa K. Adeno-associated virus (AAV) vector-mediated liver- and muscle-directed transgene expression using various kinds of promoters and serotypes. Gene ther Mol Biol 2004;8:9-18

Nomoto T, Okada T, Shimazaki K, Mizukami H, Matsushita T, Hanazono Y, Kume A, Katsura K, Katayama Y, Ozawa K. Distinct patterns of gene transfer to gerbil hippocampus with recombinant adeno-associated virus type 2 and 5. Neurosci Lett 2003;340:153-7

Ogasawara Y, Urabe M, Ozawa K. The use of heterologous promoters for adeno-associated virus (AAV) protein expression in AAV vector production. Microbiol Immunol 1998;42:177-85

Okada T, Nomoto T, Shimazaki K, Lijun W, Lu Y, Matsushita T, Mizukami H, Urabe M, Hanazono Y, Kume A, Muramatsu S, Nakano I, Ozawa K. Adeno-associated virus vectors for gene transfer to the brain. Methods 2002;28:237-47

Shevtsova Z, Malik JM, Michel U, Bahr M, Kugler S. Promoters and serotypes: targeting of adeno-associated virus vectors for gene transfer in the rat central nervous system *in vitro* and *in vivo*. Exp Physiol 2005;90:53-9

Veldwijk MR, Topaly J, Laufs S, Hengge UR, Wenz F, Zeller WJ, Fruehauf S. Development and optimization of a real-time quantitative PCR-based method for the titration of AAV-2 vector stocks. Mol Ther 2002;6:272-8

Xu L, Daly T, Gao C, Flotte TR, Song S, Byrne BJ, Sands MS, Parker Ponder K. CMV-beta-actin promoter directs higher expression from an adeno-associated viral vector in the liver than the cytomegalovirus or elongation factor 1 alpha promoter and results in therapeutic levels of human factor X in mice. Hum Gene Ther 2001;12:563-73

Yamasoba T, Suzuki M, Kondo K. Transgene expression in mature guinea pig cochlear cells *in vitro*. Neurosci Lett 2002;335:13-6

In: Genetic Vectors Research Focus
Editor: P. S. Ruiz, pp. 31-34

ISBN: 978-1-60021-952-8

Commentary E

AAV VECTORS PROVIDE A VALUABLE TOOL FOR NEUROSCIENCE

Shin-ichi Muramatsu
Division of Neurology, Jichi Medical University, Japan.

ABSTRACT

Recombinant adeno-associated virus (AAV) vectors provide efficient and long-term gene expression in the brain without significant toxicity. AAV vector-mediated expression of pathogenic genes can be used to create novel animal models of neurological diseases and spatially controlled delivery of Cre recombinase allows conditinal inactivation of target genes in adult transgenic mice. AAV vectors are faily useful in neuroscience.

Although the ultimate aim of developing new viral vectors is clinical application for safe and effective gene therapy, the expanding knowledge of vector biology make viral vector-mediated gene transfer a very efficient tool for studying complex features of the central nervous system and elucidating the pathogenesis of neurological diseases. In preclinical gene therapy experiments using animal models of neurodegenerative disorders, some of the most powerful gene delivery vehicles are recombinant adeno-associated virus (AAV) vectors, the only vectors derived from non-pathogenic and replication-defective viruses. To date, more than 100 different AAV sequences have been isolated from human and nonhuman primates, and recombinants have been investigated extensively for tissue tropism and transduction efficiency [1]. Vectors derived from AAV serotype 2 (AAV-2), a prototype of AAV, can provide long-term (>3 years) gene expression in mammalian brains without creating severe toxic effects or immune responses. Clinical trials for Parkinson's disease have been conducted using AAV-2 vectors [2] and the safety of these vectors has been confirmed [3]. While AAV-2 rarely transduces glial cells, transduction of oligodendrocytes is desirable for gene therapy of diseases that affect myelin, such as multiple sclerosis and leukodystrophy. Among the various new AAV serotypes that have been cloned recently, AAV serotype 8